DEMOCRATIC AND POPULAR REPUBLIC OF ALGERIA
MINISTRY OF HIGHER EDUCATION AND SCIENTIFIC RESEARCH
UNIVERSITY OF MOHAMED BOUDIAF - M'SILA

FACULTY OF SCIENCES
DEPARTMENT OF PHYSICS

N° :……..

DOMAIN : SCIENCE OF MATTER
FIELD : PHYSICS
OPTION : MATERIALS SCIENCE

Dissertation presented to obtain
the Degree of Academic Master

By: **Mehddeb Asma**

Entitled

Study of the structural, electronic, elastic and optical properties of the $CuFeO_2$ compound

Defended on 26 June 2018 before the jury composed of:

Pr. IBRIR Miloud	University of Mohamed Boudiaf - M'sila	Chairman
Pr. DEGHFEL Bahri	University of Mohamed Boudiaf - M'sila	Supervisor
Pr. ALLALI Djamel	University of Mohamed Boudiaf - M'sila	Examiner

Academic Year : 2017/2018

Contents

CHAPTER II :

Computational details and definition of calculated parameters

CHAPTER III :

Results & discussion

Liste Of Figures

CHAPTER I :

CHAPTER II :

CHAPTER III :

List Of Tables

CHAPTER III :

General Introduction

General Introduction:

In 1873, Friedel first noted the existence of the compound $CuFeO_2$ during the analysis of a mineral sample from Siberia [1]. The mineral was named delafossite in honor of the French mineralogist and crystallographer Gabriel Delafosse, whose work elucidated the interrelationships between crystal symmetry and physical properties. Later work by Rogers confirmed the existence of the mineral in a number of copper mines in America [2.3]. Delafossite is a secondary mineral generally found near the base of the oxidized zone of copper deposits. The crystal structure of delafossite was determined first by Soller and Thompson [4] using a synthetically prepared sample and later by Pabst [5] using a mineral sample.

The $CuFeO_2$ delafossite compound belong to a family of ternary oxides with the general formula ABO_2, which display a characteristic of a delafossite group (space group :$R\bar{3}m$). Over the past decade, materials with delafossite structures have attracted interest because of their optoelectric, electric, and thermoelectric properties.[1–6]. Among them, Cu-based materials are exceedingly studied for transparent conducting oxides (TCOs) and thermoelectric applications, for instance p-type transparent conducting oxides based on $CuFe_{1-x}Sn_xO_2$ [7] $CuNdO_2$ [8] $CuFe_{1-x}Cr_xO_2$ [9] and $CuGaO_2$ [10] and thermoelectric materials based on $CuFe_{1-x}Ni_xO_2$ [11] RCuO2 (R = Y, La, Pr, Nd, Sm, and Eu) [6] and $Cu_{1-x}Pt_xFeO_2$ [12]. The magnetic properties of delafossite oxides have also gained attention owing to their great application potential for diluted magnetic semiconductors (DMSs) [10,13,14]. Particularly applications for spintronic and transparent electron devices. However, there are few studies reported for DMSs such as $CuFe_{1-x}Rh_xO_2$ [15] $CuCr_{1-x}FexO_2$ [14,16] $CuCr_{1-x}Co_xO_2$ [13] and $CuGa_{1-x}(Ca, Mg)_xO_2$ [10].

Lately, $CuFeO_2$ has caught considerable attention owing to its multiferroic phase, where antiferromagnetism and ferroelectricity coexist, under an applied magnetic field [17, 18] or in the case of Fe^{+3} replace with nonmagnetic trivalent ions [19, 20].

After we gave an overview of $CuFeO_2$ properties and their application, the present work is devoted to present first-principles calculations of structural, elastic, electronic and optical properties of $CuFeO_2$ compound and it is organized as follows:

In the first chapter, we describe the fundamental mathematical problem needed to solve the many-body quantum mechanics for a system of nucleis and electrons where we introduce the Born- Oppenheimer and Hartree-Fock approximation, but it is not enough to solve the many body problem, so we must move to another simple and exact method, which is known as the Density functional theory (DFT) developed by Kohn-Sham which is outlined in this work. And we also introduce some approximations for electronic structure calculations (Pw+PP, APW, LAPW, PAW and APW+lo). At the end of the chapter we defines DFT as Implemented in CASTEP code (Cambridge Sequential Total Energy Package) to calculate all the properties of our compound ($CuFeO_2$)..

In the second chapter, a preview is given about Delafossite $CuFeO_2$ structure and the computational details of delafossite structural, elastic, electronic and optical properties.

The last chapter is devoted to present and discuss the obtained results of $CuFeO_2$ compound.

Finally, a brief conclusion is given about the obtained results.

REFERENCES:

[1] M.C. Friedel, C. R. Hebd. Acad. Sci, (1873), vol 77, p 211.

[2] A.F. Rogers, Am. J. Sci, (1913), vol 35, p 290.

[3] A.F. Rogers, Am. Mineral, (1922), vol 7, p 102.

[4] W. Soller, A.J. Thompson, Phys. Rev, (1935), vol 47, p 644.

[5] A. Pabst, Am. Mineral, (1946), vol 31, p 539.

[6] K. Isawa, Y. Yaegashi, S. Ogota, M. Nagano, S. Sudo, K. Yamada, and H, (1998), vol 57, p7590

[7] C. Ruttanapun, B. Boonchom, M. Thongkam, S. Kongtaweelert, C.Thanachayanont, and A. Wichainchai, J. Appl. Phys, (2013), Vol 113, p 023103.

[8] G. Dong, M. Zhang, M. Wang, F. Tang, H. Li, A. Huang, and H. Yan,J. Phys. Chem. Solids, (2012),vol 73, p 1170.

[9] M. Lalanne, A. Barnabe, F. Mathieu, and Ph. Tailhades, Inorg. Chem,(2009), vol 48, p 6065.

[10] F. Jlaiel, T. Elkhouni, M. Amami, P. Strobel, and A. B. Salan, Mater. Res. Bull,(2013) Vol 48, p 1020.

[11] J.-S. Kang, D. H. Kim, J. Hwang, E. Lee, T. Nozaki, K. Hayashi, T.Kajitani, B.-Y. Kim, and B. I. Min, Appl. Phys. Lett, (2013), Vol 99, p 012108.

[12] C. Ruttanapun, A. Wichainchai, W. Prachamon, A. Yangthaisong, A.Charoenphakdee, and T. Seetawan, J. Alloys Compd, (2011), vol 509, p 4588.

[13] T. Elkhouni, M. Amami, C. V. Colin, P. Strobel, and A. Ben Salah,J. Magn. Magn. Mater, (2013), vol 330, p 101.

[14] C. Gao, F. Lin, X. Zhou, W. Shi, and A. Liu, J. Alloys Compd, (2013), vol 565, p 154.

[15] E. Pachoud, C. Martin, B. Kundys, Ch. Simon, and A. Maignan, J. Solid State Chem, (2010), vol 183, p 344.

[16] F. Lin, C. Gao, X. Zhou, W. Shi, and A. Liu, J. Alloys Compd, (2013), vol 581,p 502.

[17] T. Kimura, J. C. Lashley, and A. P. Ramirez, Phys. Rev B , (2006), vol 73, p 220401.

[18] S. Seki, H. Murakawa, Y. Onose, and Y. Tokura, Phys. Rev. Lett, (2009), Vol 103,p 237601.

[19] S. Seki, Y. Yamasaki, Y. Shiomi, S. Iguchi, Y. Onose, and Y. Tokura, Phys. Rev B , (2007), vol 75, p 100403.

[20] N. Terada, T. Nakajima, S. Mitsuda, H. Kitazawa, K. Kaneko, and N. Metoki, Phys. Rev B, (2008), vol 78, p 014101.

CHAPTER I :

DFT and CASTEP code

CHAPTER I:

DFT and CASTEP code

I.1 Background:

One of the most challenging problems in condensed matter physics computational materials physics is to describe the electronic structure of many-body systems. Thus, numerical computational is becoming an essential tools in condensed matter physics and material science due to their ability to describe the material properties. Over the past few decades several models are used to describe the electronic structure of atoms and molecules. The electronic Schrödinger equation is a very accurate ab-initio model but unfortunately, it is difficult to deal with it numerically. Therefore, we need an approximation to solve this problem. This reality prompts two kinds of methodologies; the first one is based on the wave function description and the second approach is the DFT formed by Hohenberg and Kohn which depends on the electron density. The following chapter is a brief overview of Density Functional Theory, and its role in solving the quantum mechanical problems [1].

I.2 The Many-Body Problem:

All materials are composed of atomic nuclei and electrons [2]. So, according to quantum mechanics the energy and the behavior of electrons and nuclei can be predicted by solving the non-relativistic Schrödinger equation for the system:

$$H\Psi = E\Psi \tag{I.1}$$

Where E is the energy of the system and H is the Hamiltonian of the system given in Eq (I.2):

$$H = -\frac{1}{2}\sum_{i=1}^{N}\frac{1}{m_e}\nabla^2_i - \frac{1}{2}\sum_{A=1}^{M}\frac{1}{M_A}\nabla^2_A + \sum_{i=1}^{N}\sum_{j>i}^{N}\frac{1}{r_{ij}} + \sum_{A=1}^{M}\sum_{B>A}^{M}\frac{Z_A Z_B}{R_{AB}} - \sum_{i=1}^{N}\sum_{A=1}^{M}\frac{Z_A}{r_{iA}} \quad \text{(I.2)}$$

- The first two terms are the kinetic energies of *N* electrons with masses m_e and *M* nuclei with masses M_A.

- The third term is the electrostatic repulsion between electrons.

- The fourth term is the electrostatic repulsion between nuclei.

- The last term is the Colombian attraction between electrons and nuclei.

This Hamiltonian can be decomposed in five terms;

$$H = T_n + T_e + V_{N-N} + V_{e-e} + V_{N-e} \quad \text{(I.3)}$$

In practice, it is only possible to solve the Schrodinger equation exactly for small simple systems such as the hydrogen atom. For larger systems like molecules and solids, additional approximations have to be made.

I-3 Born – Oppenheimer approximation:

In 1927 Born and Oppenheimer was made an approximation [3] which based on the fact that the nuclei are much heavier than the electrons, therefore wave functions of electrons and atomic nuclei can be separated [4].

$$\Psi = \psi_{electrons} \times \psi_{nuclei} \quad \text{(I.4)}$$

Due to the fact that the kinetic energy of nuclei are much smaller than the electron one, the fourth term is a constant and is included in the total energy after calculating the wave function.

$$E_{tot} = E_{electrons} + E_{nuclei} \quad \text{(I.5)}$$

Hence, the solution of the Schrodinger equation with H_{elec} is to find the electronic wave function ψ_{elec} and the electronic energy E_{elec}.[4].

$$H_{elec}\psi_{elec} = E_{elec}\psi_{elec} \quad \text{(I.6)}$$

Within this approximation, the Hamiltonian of the system can be written as:

$$H_e = -\sum_{i=1}^{N} \frac{1}{2}\nabla^2_i + \sum_{i=1}^{N}\sum_{j>i}^{N} \frac{1}{r_{ij}} - \sum_{i=1}^{N}\sum_{A=1}^{M} \frac{Z_A}{r_{iA}} = T_e + V_{N-e} + V_{e-e} \quad \text{(I.7)}$$

The conceptual and numerical problems related to the electron-electron interactions (second term) in Equation (I.7) are the most challenging to deal with.We have reduced the complexity of the problem. But, the solution of equation (I.7) remains always difficult. Thus, we have to make other approximations to solve this problem.

I.4 The Hartree approximation:

The simplest way to solve the many-electron equation [5] is to rewrite Eq (I.6) as a one-particle equation for an electron moving in an average potential from all the electrons as proposed by Hartree, The second term in Equation (I.7) can therefore be approximated as a sum of one-electron potentials V_i where ψ_i is the orbital for the electron as shown in Eq (I.8):

$$\sum_{i\neq j}^{N} \frac{1}{r_{ij}} \approx \sum_{i=1}^{N} V_i\,(r_i) = \sum_{i=1}^{N} \frac{\int n(r_j) - |\psi_i(r_j)|^2}{|r_i - r_j|} dr_j \quad \text{(I.8)}$$

To actually calculate the Hartree potential it is necessary to know the electronic charge distribution of the system. If the electrons are assumed to be independent of each other, then it is straightforward to construct *n(r)* from the single electron eigenstates .The total wavefunction is not antisymmetric with respect to the exchange of electrons and does not respect the Pauli's exclusion principle. To introduce Pauli's exclusion principle we must go beyond Hartree method [5].

I.5 The Hartree-Fock approximation:

Hartree-Fock method [4, 6] is commonly used to solve many-body problem in quantum mechanics, where in the case of many-electron system the method based on an approximation to the ground state wave function Ψ_0 for N electrons by antisymmetric product of N orthonormal single-electron wave function ψ_i . The antisymmetry of the approximate wave function Ψ_{HF} is ensured by the form of the Slater determinant as shown in Eq (I.9):

$$\Psi_0 \approx \Psi_{HF} = \frac{1}{\sqrt{N!}} \begin{vmatrix} \psi_1(r_1) & \psi_2(r_2) & \cdots & \psi_N(r_1) \\ \psi_1(r_2) & \psi_2(r_2) & \cdots & \psi_N(r_2) \\ \vdots & \vdots & \ddots & \vdots \\ \psi_1(r_N) & \psi_2(r_N) & \cdots & \psi_N(r_N) \end{vmatrix} \quad \text{(I.9)}$$

The minimum point of the Hartree-Fock energy functional is the ground state wave function

$$E[\Psi] = \langle \Psi | H | \Psi \rangle \quad \text{(I.10)}$$

Thus, the energy is given by the formula in Eq (I.11):

$$E_{HF} = \sum_{i=1}^{N} H_i + \frac{1}{2}\sum_{i,j=1}^{N}(J_{ij} - K_{ij}) \quad \text{(I.11)}$$

$$\text{Where: } \begin{cases} H_i = \int \psi^*{}_i(r)\left[-\frac{1}{2}\nabla^2{}_i + V_{ext}(r)\right]\psi_i(r)dr \\ J_{ij} = \iint \psi_i(r_1)\,\psi^*{}_i(r_1)\frac{1}{r_{12}}\psi^*{}_j(r_2)\,\psi_j(r_2)\,dr_1 dr_2 \\ K_i = \iint \psi*(r_1)\,\psi^*{}_j(r_1)\frac{1}{r_{12}}\psi_i(r_2)\,\psi*(r_2)\,dr_1 dr_2 \end{cases} \quad \text{(I.12)}$$

- H_i defines the contribution due to the kinetic energy and the electron-nucleus attraction.

-J_{ij} are called Coulomb integrals.

- The K_{ij} are called exchange integrals.

The electronic correlation is totally absent in the theory HF. Although the treatment is correct, to include the correlation, it is necessary to go beyond the HF theory [5].

I.6 The correlation energy:

The Hartree-Fock approach suppose that, the true many-body problem can be approximated as independent electrons in an effective potential, the energy missing is defined as the *correlation* energy ($E_{corr} = E + E_{HF}$). There are different methods which take correlation effects into account, for instance Møller-Plesset (MP) perturbation theory [7], configuration interaction (CI) [8] and coupled cluster (CC) methods [9] or quantum Monte-Carlo methods. However, these methods are computationally very expensive and only the

smallest systems can be currently computed. On the other hand, DFT theory offers a good compromise between the qualitative description of electronic structure and the computational effort required to produce the result. Thus, DFT is one of the most popular and successful quantum mechanical approaches to describe matter.

I.7 Density functional theory:

Density functional theory (DFT) is a mathematical tool for solving problems in many-body systems. One of the main reasons for the successful and popularity of DFT lies in its excellent compromise between accuracy and feasibility. In DFT [10] the ground state energy of a system can be expressed solely as a function of the ground state charge density where the *N*-electron wave function are replaced by the simpler electron density (*n*).

$$n(r) = |\Psi(r_1, s_1; \dots \dots; r_N, s_N)|^2 \quad \text{(I.13)}$$

Where $r_i$and $s_i$are the positon and spin of the electron.

This approach can reduce complexity of calculation because electron density is a function for just three variables while wave function is a function of 3N variables [11].

I.7.1 The Thomas-Fermi theory:

The predecessor to DFT was the Thomas-Fermi model proposed by Thomas [12] and Fermi [13] in 1927. In this method they introduced the concept of using the electron density rather than the wavefunction, while the kinetic energy is approximated as an explicit functional of density based on non-interacting electrons in a homogeneous gas.

The kinetic energy of electrons within this model is given by:

$$T[\, n(r)] = C_F \int n^{5/3}(r) dr \quad \text{(I.14)}$$

With: $C_F = \frac{3}{10}(3\pi^2)^{2/3}$ =2.871 and n(r) defines the density of electron and by the integration of n(r) the total number of electrons N is:

$$\int n(r) dr = N \quad \text{(I.15)}$$

Within this model and by neglecting the exchange and correlation terms, Thomas-Fermi (TF) total energy of an atom with a nuclear charge Z is given by :

$$E_{TF}[n(r)] = C_F \int n^{5/3}(r)dr - Z\int \frac{n(r)}{r}dr + \frac{1}{2}\iint \frac{n(r)-n(r')}{|r-r'|} \quad \text{(I.16)}$$

The second and third terms correspond to the electron-nucleus and the Coulomb part of the electron-electron interactions respectively.

The TF model considered as an oversimplified model due to the poor description of the uniform gas in the representation of the kinetic energy, and also the complete neglect of exchange and correlation terms in the electron-electron interaction.

I.7.2 The Hohenberg-Kohn Theorems:

In 1964 Hohenberg and Kohn [14] proposed two theorems, building the basis of modern DFT as it is applied today:

Theorem 1:

The first theorem states that [15] any system's ground-state density n(r) uniquely determines the external potential applied to the system. Therefore, the complete Hamiltonian is uniquely determined by the ground state particle density.

Proof:

In principal suppose there is an exact ground state density n(r) non degenerate, and apply two different external potentials V_{ext} (r) and v'_{ext}(r) but lead to the same ground state density n_0(r). The two external potentials would give two different Hamiltonians, hence two different ground state wave functions [15]:

$$V_{ext}(r) \rightarrow H \rightarrow \psi \rightarrow E_0$$

$$V'_{ext}(r) \rightarrow H' \rightarrow \psi \rightarrow E_0$$

It follows that:

$$\begin{aligned} E_0 &< \langle \psi' | H | \psi' \rangle \\ &< \langle \psi' | H' | \psi' \rangle + \langle \psi' | H - H' | \psi' \rangle \\ &< E_0 + \int n^0(r)[Vext(r) - V'ext(r)]\, dr \end{aligned} \quad \text{(I.17)}$$

The same:

$$\begin{aligned} E_o &< \langle \psi | H' | \psi \rangle \\ &< \langle \psi | H | \psi \rangle + \langle \psi | H' - H | \psi \rangle \\ &< E_0 + \int n_0(r)[Vext(r) - Vext(r)]dr \end{aligned} \quad \text{(I.18)}$$

Adding Eq (I.17) +Eq (I.18): $E_0 + E'_0 < E'_0 + E_0 \rightarrow$ fall into contradiction.

So, it is impossible that two different external potentials V_{ext}(r) [15] give the same ground state density n_0(r). That means there is a relationship between the ground state density n_0(r) and the external potential V_{ext}(r).

Theorem 2:

A universal functional for the energy E[n] in terms of the density n(r) can be defined valid for any external potential V_{ext}(r). The exact ground state energy of the system is the global minimum of this functional and the density $n(r)$ that minimizes the functional is the exact ground-state density n_0 (r). So, the exact ground state energy and density are, completely determined by the functional E[n(r)] [15]:

$$E[\text{n(r)}] = \int n(r)Vext(r)dr + F[n(r)] \quad \text{(I.19)}$$

The universal HK functional can be written as:

$$F[\text{n(r)}] = T[n\ (\text{r})] + E_{int}n(\text{r})] \quad \text{(I.20)}$$

F_{HF}[n] included the kinetic energy T[n(r)] and the interaction energy of the particles E_{int}[n(r)]

Proof:

According to variational principle the energy functional $E[\Psi']$, for any wavefunction Ψ' is:

$$E[\Psi'] \equiv \langle \Psi' | T + V_{int} + V_{ext} | \Psi' \rangle \quad \text{(I.21)}$$

When $\Psi'$is the ground state wavefunction Ψ_0, E[Ψ'] has the global minimum value and the total number of the particles is conserved. As denoted in first HK theorem Ψ'must correspond to a ground state with particle density $n'(r)$and external potential $V'_{ext}(r)$, thus E [Ψ'] is a functional of $n'(r)$[15].

According to variational principle:

$$\begin{aligned} \text{E } [\psi'] &\equiv \langle \psi' | T + Vint + Vext | \psi' \rangle \\ &= \text{E } [n'(r)] \\ &= \int n'(r) V'ext(r) dr + F[n'(r)] \\ &> E[\psi_0] \\ &= \int n(r) Vext(r) dr + F[n(r)] \\ &= \text{E } [n_o(r)] \end{aligned} \quad \text{(I.22)}$$

Therefore the energy functional rated for the correct ground state density $n_0(r)$ is indeed lower than the value of this functional for any other density $n(r)$. The universal functional within HK theorems $F[n$ (r)] is unknown. So, it is still impossible to calculate any property of a system. This difficulty was beat by Kohn and Sham when they proposed the outstanding known Kohn-Sham method. [15]

I.7.3 Kohn-Sham method:

Later in 1965 after Hohenberg and Kohn published their work on the representability of the external potential by the particle density, Kohn and Sham [16] introduced a method by proposing the following assumptions:

First, a system of interacting electrons is mapped onto an auxiliary system of non-interacting electrons having the same ground state charge density n(r) as the interacting system.

Second, the auxiliary Hamiltonian is chosen to have the usual kinetic operator and an effective potential V_{eff}(r).

The Hamiltonian of the system [11] defined in this manner can be written as:

$$H = T_s + V_s \tag{I.23}$$

The energy of this system according to Hohenberg-Kohn theory can be written as:

$$E[n(r)] = T_s[n(r)] + \int V_s(r)n(r)dr \tag{I.24}$$

The electron density of the non-interacting system of electrons can be counted by summing over all occupied single-particle orbitals:

$$n(r) = \int_{i=1}^{N} |\phi_i(r)|^2 \tag{I.25}$$

The energy functional for the real system can be described to include the kinetic.

$$E[n(r)] = T_s[n(r)] + E_{xc}[n(r)] + \int V_s(r)n(r)dr + \iint \frac{n(r)n(r')}{|r-r'|} drdr' \tag{I.26}$$

Where $E_{xc}[n(r)]$ is the exchange-correlation energy. Thus, we can get Kohn-Sham equations by applying the variational principle:

$$\left[-\frac{\hbar^2}{2m_e}\nabla^2_i + V_H(r) + V_{ext}(r) + V_{xc}(r)\right]\phi_i(r) = \epsilon_i\phi_i \tag{I.27}$$

Where $\underbrace{V_{xc} = \frac{\partial E_{xc}[n(r)]}{\partial n(r)}}_{\text{The exchange-correlation potential}}$ (I.28)

The solely unknown left is the exchange-correlation energy functional E_{xc} . There is no exact form for it, but Kohn and Sham in their work proposed a local density approximation and also suggested an improvement using a gradient extension [11].

I.7.4 Exchange and Correlation approximations:

There are different methods to calculate the exchange and correlation term E_{xc}[n] ,for instance the Local Density Approximation (LDA) and the Generalized Gradient approximation (GGA) , meta GGA and hybrid functional[17].

I.7.4.1 The Local Density Approximation (LDA):

Already in their original work, Kohn and Sham proposed a local density approximation (LDA). This approximation based on that the exchange-correlation energy of an inhomogeneous electron system, is approximated by that of a homogeneous electron gas.[17].

For spin-unpolarized system the exchange-correlation energy can be written as:

$$E_{xc}^{LDA}[n] = \int n(r)\varepsilon_{xc}(n)dr \quad \text{(I.29)}$$

The exchange part for the homogeneous electron gas is known analytically as:

$$\varepsilon_{xc}(n) = -\frac{2}{3}\left(\frac{3}{\pi}n(r)\right)^{1/3} \quad \text{(I.30)}$$

For the spin-polarized, the exchange-correlation energy in the local spin density approximation (LSDA) can be written as:

$$E_{xc}^{LSDA}[n_\alpha, n_\beta] = \int n(r)\varepsilon_{xc}(n_\alpha n_\beta) \quad \text{(I.31)}$$

n_α, n_β Are the electronic densities of spin.

I.7.4.2 The Generalized Density Approximation (GGA)

The Generalized Gradient Approximation (GGA) [17] improves the LDA method by considering the system as a non-uniform electron gas and taking account of non-local electron effects in the functional. The exchange-correlation term can be written as a function of *n* and it derivative ∇n :

$$E_{xc}^{GGA}[n] = \int \varepsilon_{xc}(r)[n(r) + \nabla n(r)]d^3r \quad \text{(I.32)}$$

The GGA group includes BLYP, PW91, and PBE … etc, can be generated by using approximations for the above equation. GGA allows for a larger fluctuation than LDA, that's why the GGA generally gives better results than LDA.

I.7.4.3 Meta GGA:

The Meta-GGA [17] go one step further than GGA functionals, by adding the second derivative of electron density or more recently, the kinetic energy density τ :

$$\tau(r) = \sum_i \frac{1}{2} \left|\nabla \varphi_i(r)\right|^2 \quad \text{(I.33)}$$

Where the exchange-correlation term can be written as:

$$E_{xc}^{meta\ GGA}[n] = \int \varepsilon_{xc}(r)[n(r) + \nabla n(r) + \tau(r) d^3 r \quad \text{(I.34)}$$

TPSS functional is one of the amongst commonly utilized meta-GGA functionals, developed by Tao, Perdew, Staroverov and Scuseria.

I.7.4.4 The hybrid functionals:

The next successful alternative in the development of the exchange-correlation functionals was the inclusion of the Hartree-Fock exact exchange term in the calculation of E_{xc} , Hybrids can be formalize in terms of what is called Generalized Kohn-Sham Theory[18], for instance the most commonly used hybrid functional is B3LYP[19] the exchange - correlation part can be written as :

$$E_{xc}^{B3LYP} = E_{xc}^{LDA} + a_0(E_x^{HF} - E_x^{LDA}) + a_x(E_x^{GGA} - E_x^{LDA}) + E_c^{LDA} + a_c(E_c^{GGA} - E_c^{LDA)} \quad \text{(I.35)}$$

E_x^{GGA} And E_c^{GGA} are the generalized gradient approximation exchange and correlation functionals and E_c^{LDA} is the local density approximation to the correlation functional, a_0 is set to 0.20, a_x is set to 0.72, a_c is set to 0.81.

I.8 Electronic band structure method:

Computational in an isolated system containing few atoms is straightforward, but often it is required to computational a bulk solid material which contains a great many atoms. However, this can be avoided by using the periodicity of the solids crystal structure. Thus, to reduce the problem to only those electrons and ionic cores that are contained in the unit cell,

which forms the smallest repeat unit. Therefore, to calculate the electron eigenstates for solid it's necessary solving the Kohn-Sham Hamiltonian for the atoms in the unit cell. The effective potential, in the Kohn-Sham equation will be now periodic $V_{eff} = V_{eff}(R + r)$ for all lattice vectors R of the crystal [20].

Bloch's theorem [20] states that the eigenstates ϕ of a one-particle can be written as the product of a plane wave and a lattice periodic function

$$\phi_{nk}(r) = e^{ikr} U_{nk}(r) \tag{I.36}$$

K is the wavevector and can be picked in the main Brillioun zone because of the translational symmetry, and *n* is the band index which determines different solutions for a given k, $U_{nk}$is a function with the periodicity of the lattice.

$$U_{nk}(r) = U_{nk}(r + R) \tag{I.37}$$

The E_{nk+G} is an eigenvalue for all vectors G of the reciprocal lattice. If E_{nk} is an energy eigenvalue;

$$E_n(k) = E_n(k + G) \tag{I.38}$$

Thus the energy values are periodic in reciprocal space. Now, it is clear that the problem of solving K-S equation has been reduced to that of calculation of infinitely many k-points inside the unit cell.

I.8 Methods for electronic structure calculation:

The most three prevalent methods used to compute the electronic band structure are : pseudopotentials in combination with the plane wave basis set, the linearized augmented plane wave (LAPW) method and the projector augmented wave (PAW) method [20].

I.8.1 Plane wave pseudo-potential method:

Plane waves [20] are in sense, the ideal basis functions for a periodic system where the extended periodic functions $U_{nk}(r)$ can be written as:

$$U_{nk}(r) = \sum_G C_{nk,G}\, e^{iGr} \tag{I.39}$$

Thus the addition is over all the reciprocal lattice vectors G of the system under study. The electronic wave functions can be written as:

$$\phi_{nk}(r) = \sum_G C_{nk,G} e^{i(k+G)r} \quad \text{(I.40)}$$

Now the electronic wavefunctions at every k-point are expressed in terms of a discrete Fourier series plane wave basis set. This Fourier series is infinite where in practice we can't work with an infinite basis set. This problem can be solved, by setting an upper boundary to the kinetic energy of the plane waves. This limit is called energy cut-off [20] E_{cut} . The effect of the cut-off is to produce a less accurate wavefunction and hence a higher energy of the system.

$$\frac{|K+G|^2}{2} < E_{cut} \quad \text{(I.41)}$$

Although DFT greatly simplifies the complexities of electronic-structure calculations of solids, but for systems with a large number of electrons it still remains computationally very costly. Here, pseudo-potentials [17] helped in a definitive way to make the calculations easy by using the fact that the physical properties of solids depend primarily on valence electrons. The pseudo-potential approximation based on those electrons in solids can be divided into core and valence electrons pseudo-potential uses this advantage and replaces the core electrons and strong ionic potential with a weaker pseudopotential that acts on a set of pseudo wave functions in place of the true valence wave function.

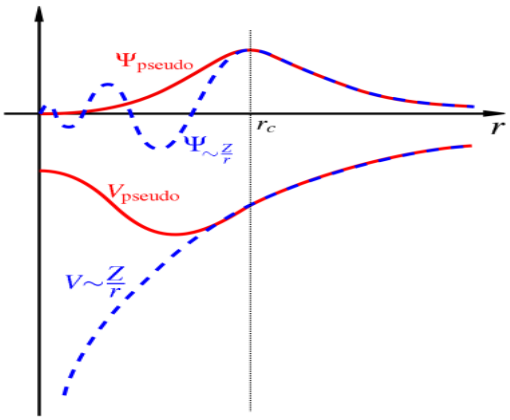

Figure I.1: Schematic representation of pseudopotential and the pseudo wave function [17].

Pseudo-potentials can be generated by different schemes. Some of pseudo-potentials belongs to the norm-conserving pseudo-potential, which enforce the condition that, outside of a cut-off radius, the norm of each pseudo-wavefunction is identical to its corresponding all-electron wavefunctions [21].

Norm-conserving pseudopotentials are formed such that they satisfy the following general conditions [22]:

1) The valence pseudo-wavefunctions generated from the pseudopotential contain no nodes
2) beyond a chosen cut-off radius, the normalized radial all-electron wavefunction (AE) = The normalized atomic radial pseudo-wavefunction (PP)

$$R^{PP}{}_{l}(r) = R^{AE}{}_{l}(r) \quad for\ r > r_c \tag{I.42}$$

3) for the above two wavefunctions, The charge enclosed within $r_c$must be equal :

$$\int_0^{r_c} |R^{PP}{}_{l}(r)|^2 r^2 dr = \int_0^{r_c} |R^{AE}{}_{l}(r)|^2 r^2 dr \tag{I.43}$$

4) The valence all-electron and pseudopotential eigenvalues must be equal

$$\varepsilon^{PP}{}_{l} = \varepsilon^{AE}{}_{l} \tag{I.44}$$

There is another type of pseudopotentials which is the ultrasoft pseudo-potentials. In 1990, Vanderbilt [23] constructed a new class of pseudo-potentials in order to greatly reduce the cut-off energy needed to describe localized orbitals. This new class of pseudo-potentials is characterized by pseudo-wave functions that can be arbitrarily smooth in the core region and for this reason that these are called "ultra-soft pseudo-potentials". On the other hand, this new class of pseudo-potentials allowed the use of a larger cutoff radius than that approach for pseudo-potentials with conserved norms.

Vanderbilt has imposed its pseudo-potentials as a solution to the problem of the use of the pseudo-potential with conserved norm, which consists in admitting a very large number of plane waves for the description of the electrons. Consequently, a cut-off-radius R_C is relatively weak.

In short, Vanderbilt was able to make its pseudo-potentials more advantageous than that of the conserved standard. Recapping the benefits of ultra-soft Vanderbilt :

- ✓ They are much softer than standard-conserved potentials, a direct consequence of better transferability and accuracy than for other pseudo-potentials [24].
- ✓ Ultra-soft potentials usually treat shallow heart conditions as valences. This also adds to the accuracy and high transferability of potentials [25].

There is another methods to solve the Kohn-Sham equations without using pseudopotential. These methods are called all-electron methods (APW, LAPW and PAW) in which all the electrons are explicitly used in the calculation [20].

I.8.2 Augmented plane wave method (APW):

The APW method uses a different basis sets in two different regions, in which the whole space has been divided into muffin-tin (MT) spheres (spheres centered at each atomic site) and interstitial (I) region (see (Fig. (I.2)a). In the two types of regions different basis sets are used (see Fig. (I.2)b) [23].

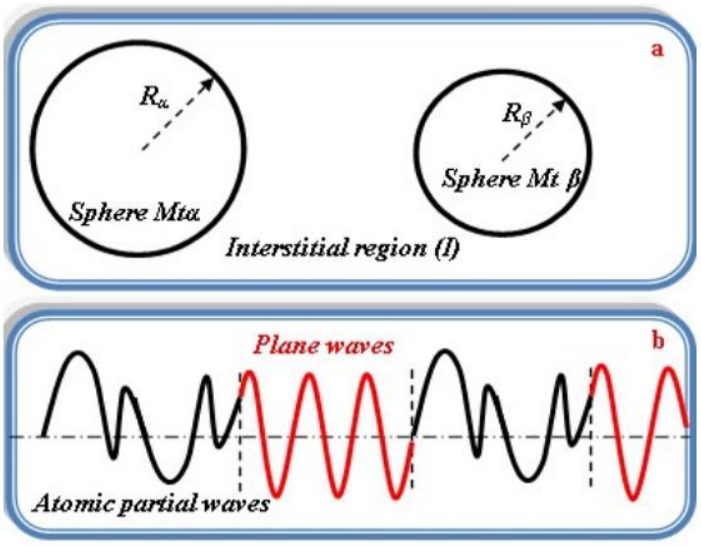

Figure I.2: Schematic division of (a) space into Muffin-tin spheres and an interstitial region. (b) Wave function; black atomic partial waves in the MT sphere and red plane waves in I region [23].

The different basis sets used in the two types of regions are:

$$\phi_{Kn}^{APW}(r,\epsilon_l) = \begin{cases} \sum_{lm} A_{lm,kn}\, U_l(r,\epsilon_l) Y_{lm}(r) \\ \frac{1}{\sqrt{\Omega}} e^{ikn,r} \end{cases} \quad \text{(I.45)}$$

Where Ω represents the cell volume, and U_l is the atomic radial function, Y_{lm} Spherical harmonic. The biggest disadvantage in the APW method is the unknown factor ϵ_l, where the APW cannot get the eigenvalues from a single diagonalization. To avoid this problem we need to describe the eigenstate $\psi_K(r)$ to get the exact value, but the resulting eigenvalue problem is non-linear in energy. So, it needs to be solved self-consistently which makes the APW method computationally inefficient.

I.8.3 Linearized Augmented Plane Wave (LAPW) method:

To avoid the non-linearity problem in the APW technique, the LAPW [20] method was developed. The radial wavefunction can be extensive in a Taylor series expansion around ϵ_i as:

$$u_l(r,\epsilon_l) = u_l(r,\epsilon_l^1) + (\epsilon_l - \epsilon_l^1)\mathring{u}_l(r,\epsilon_l^1) + O((\epsilon_l - \epsilon_l^1)^2) \quad \text{(I.46)}$$

Where $\mathring{u}_l = \frac{\partial u_l}{e^{\partial E_l}}$ and ϵ_l^1 is set near ϵ_l the radial function and energy errors are negligible. Thus, the LAPW basis set can be written as:

$$\phi_{kn}^{LAPW}(r) \begin{cases} = \sum_{lm} [A_{lm,kn}\, u_l(r,\epsilon_l) + B_{lm,kn}\mathring{u}_l(r,\epsilon_l)]\, Y_{lm}(r) \\ \frac{1}{\sqrt{V}} e^{ikn,r} \end{cases} \quad \text{(I.47)}$$

The basis set in the interstitial region is the same as in the APW method, but the basis functions in the Muffin-Tin spheres depend on u_l, and also on its energy derivative $\mathring{u}_l$. The coefficients A_{lm} and B_{lm} are determined by requiring that this basis function matches each plane wave (PW) which is the corresponding basis function of the interstitial region. Consequently, LAPW method offers more flexibility than the APW method in the Muffin-Tin spheres.

I.8.4 The APW+lo method:

Another alternative approach was proposed to avoid the non-linear problem that complicated the APW method. The new scheme was named the APW+lo (local orbitals) [20]. In APW+lo method the basis set is energy independent and it has the same basis size as the original APW method the local orbitals are added to allow an adequate variational flexibility, which can be defined as:

$$\phi^{lo}{}_{lm}(r) = \begin{cases} [A_{lm}u_l(r,\epsilon_l) + B_{lm}\mathring{u}_l(r,\epsilon_l)] & (r \in MT) \\ 0 & (r \in I) \end{cases} \quad \text{(I.48)}$$

The two coefficients $A_{lm}$and $B_{lm}$are determined by normalization and by the condition that the local orbital is zero at the Muffin-Tin boundary. The feature of the APES+lo method lies in the Combination between the accuracy in LAPW method and small basis set like the APW method [20].

I.8.5 Projector augmented wave method (PAW):

The Projector-Augmented wave (PAW) method was introduced by Peter Bloch [24] in 1994. The PAW was developed to enhance the precision and computational efficiency of the plane wave pseudopotential approach and to supply the correct wave functions, instead than the fictitious wave functions provided by the pseudopotential approach. But, it uses a decomposition of the all-electron wave function in terms of a smooth pseudo-wave function, and a rapidly varying contribution localized within the core region.

I.9 The band gap problem in DFT:

DFT is used in the electronic structure calculation of solids, molecules or atoms [20]. Electron density is the key factor from which the ground state properties are determined. It offered information about forces and stresses, which can in turn allow structural relaxation of the system. Depending on the exchange correlation functional used, DFT precisely predicts equilibrium atomic positions and lattice parameters, but it fails in the prediction of band gap and excitation energies. The band gaps calculated within DFT shown a sharp underestimation compared to experiment as shown in from Fig (I.3). The DFT underestimation of band gap is however, not surprising because DFT- KS eigenvalues are completely artificial.

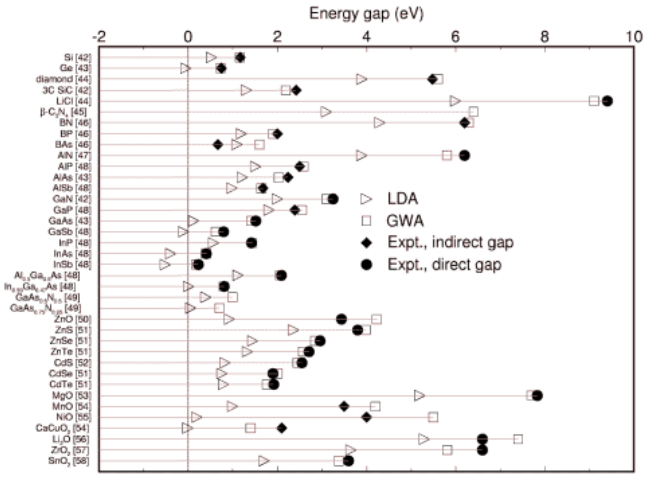

FigureI.3: Comparison between the experimental gap and the gap calculated using DFT-LDA for semiconductors and insulators [20].

There is no physical basis to interpret the Kohn-Sham gaps as the real experimental gaps, but in practice such a comparison of the band structure was motivated by the similarity of Kohn-Sham band structure and the real band structure for many systems. In semiconductors, the band gaps E_g are differences of ground-state energies (E) of N and N ± 1 particle systems:

$$E_g = E(N+1) + E(N-1) - 2E(N) = I - A \tag{I.49}$$

I represents the ionization potential and A represents the electron affinity of the system

Where

The lowest conduction band energy is :

$$\epsilon_c = E_{N+1} - E_N \tag{I.50}$$

The highest valence band energy is :

$$\epsilon_v = E_N - E_{N-1} \tag{I.51}$$

Thereby, the energy gap is related to the eigenenergies as:

$$E_g = \epsilon_{N+1}(N+1) - \epsilon_N(N) \tag{I.52}$$

Thus, it is different from the unsophisticated definition of the band gap in terms of only N-particle eigenenergies given by:

$$\epsilon_g = \epsilon_{N+1}(N) - \epsilon_N(N) \tag{I.53}$$

This variation is given by :

$$\Delta_{xc} = \epsilon_{N+1}(N+1) - \epsilon_{N+1}(N) \tag{I.54}$$

It is illustrated schematically in Fig (I.4)

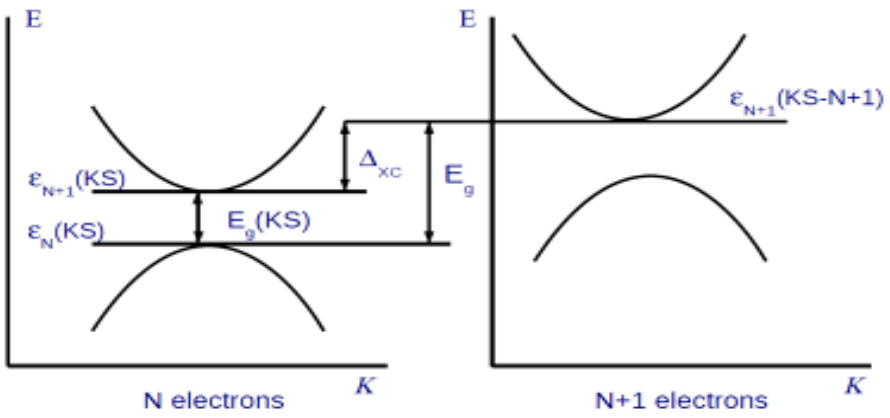

Figure I.4: Schematic illustration of the experimental band gap and Kohn-Sham gap[20].

Δ_{xc} is given by :

$$\Delta_{xc} = \lim_{\eta \to 0} \left(\frac{\delta E_{xc}}{\delta n(r)}\Big| - \frac{\delta E_{xc}}{\delta n(r)}\Big| \right) \tag{I.55}$$

The evaluation of the exchange correlation $\frac{\delta E_{xc}}{\delta n(r)}$ at the point $(N \mp \eta)$ is to ensure that this discontinuity is captured at an integer particle number (N). In LDA and GGA the value of $\Delta_{xc}$is always zero. The fundamental gap obtained from these approximations is always purely KS gap, which is the reason why their gap is all the times underestimated when compared with experimental band gap.

I.10 DFT as Implemented in Codes:

I.10.1 CASTEP code:

In this work the DFT calculations are performed using CASTEP code (Cambridge Sequential Total Energy Package) [25]. It is developed in the Theory of Condensed Matter Group at Cambridge University UK to calculate the properties of materials from first principles. It employs density functional theory (DFT) to simulate the properties of solids, interfaces, and surfaces for a wide range of materials classes such as ceramics, semiconductors and metals.

I.10.2 How Does CASTEP work?

CASTEP [26, 27] uses a total energy planewave pseudopotential method. Combining the use of pseudopotentials and plane wave basis sets makes it extremely easy to calculate the forces on the atoms, enabling efficient optimization of ionic configurations of molecules, solids, surfaces, and interfaces. In the mathematical model of the material CASTEP replaces ionic potentials with effective potentials acting only on the valence electrons in the system where electronic wavefunctions are extended through a planewave basis set, and exchange and correlation effects in electron-electron interactions can be included within either the local density (LDA) or generalized gradient (GGA) approximations.

I.10.3 Capabilities of CASTEP:

CASTEP [28] is capable to compute physical properties ; electronic properties such as band gaps, density of states and Schottky barriers; optical properties such as reflectivity, absorption, IR spectra, and dielectric functions; elastic properties,...etc. it also can reduce the complexity of calculation.

Two algorithms SCF (Self-consistent Field (see Fig (I.5)) is implemented in the Castep code to find the ground-state wavefunctions and density which are the lowest-energy solutions to the Kohn-Sham equations: the first density mixing (DM)[29] is a fast but potentially unstable method. DM method compute the ground-state wavefunctions and density separately, the Kohn-Sham wavefunctions are first computed for a given input density, and then a separate "density mixing" algorithm is used to calculate an estimate of the ground-state density. This estimate is then used as the input density for a new iteration of the method. When the ground

state has been reached, the algorithm stops because the estimated ground-state density is the same as the input density.

The second ensemble density functional theory [29] (EDFT) is a stable, but slow method of solving the Kohn-Sham equations, where in EDFT the density is always calculated directly from the estimated ground-state wavefunctions, and these wavefunctions are only ever updated in a way which brings them nearer to the ground state.

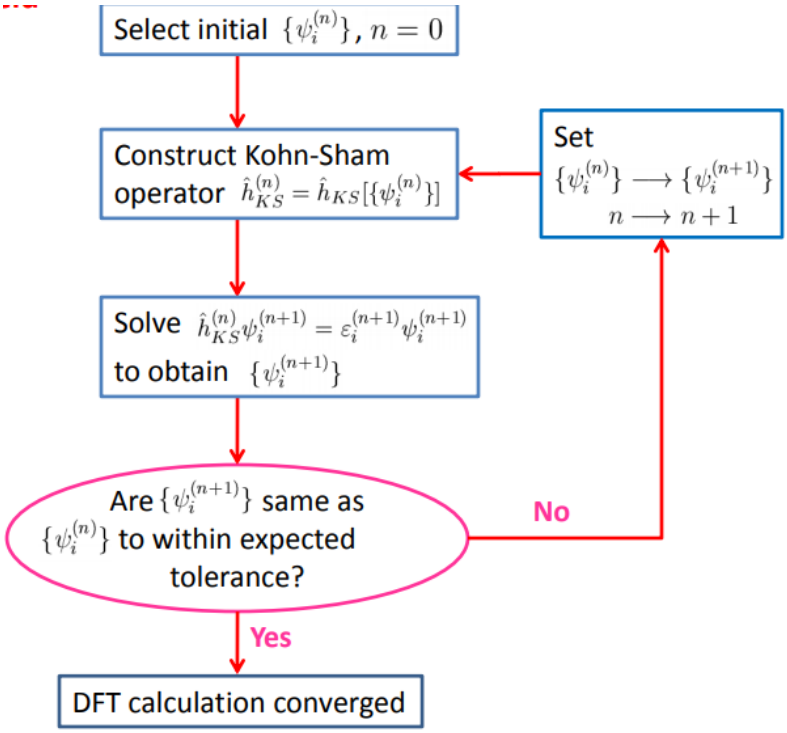

Figure I.5: Schematic illustration of Self-consistent Field (SCF)[30].

REFERENCES:

[1] Ondzibou, Ninon Gildas. *Computational study of structural, electronic and optical properties of Molybdenum Chalcogenides*. 2014. Thèse de doctorat. University of the Witwatersrand, Johannesburg

[2] Charpentier, Thibault. Détermination et calcul premiers principes, par la méthode PAW/GIPAW, de paramètres RMN de fluorures inorganiques. 2014. Thèse de doctorat. Université du Maine.

[3] M. Born and R. Oppenheimer, Annalen der Physik 84, 457 (1927).

[4] CUEVAS, Juan Carlos. Introduction to density functional theory. *Universität Karlsruhe, Germany*, 2010.

[5] Mishra, Deepti. Structural, conformational and reactivity studies on DNA base pairs and phospholipids using density functional theory (DFT). 2014. Thèse de doctorat. CSIR-National Chemical Laboratory, Pune, India.

[6] D. R. Hartree. The wave mechanics of an atom with a non-coulomb central field.part i. theory and methods, *Math. Proc. Cambridge*, (1928), vol 24, no1, p 89–110.

[7] Moller, Chr et Plesset, Milton S. Note on an approximation treatment for many-electron systems, *Physical Review*, (1934) , vol. 46, no 7, p 618.

[8] Sherrill, C. David et Schaefer III, Henry F. The configuration interaction method: Advances in highly correlated approaches. In : *Advances in quantum chemistry*. Academic Press, (1999), vol 34, p143-269.

[9] Bartlett, Rodney J. Coupled-cluster approach to molecular structure and spectra: a step toward predictive quantum chemistry. The Journal of Physical Chemistry, (1989), vol 93, no 5, p 1697-1708.

[10] Brincat, Nick. Density Functional Theory Investigation of the Uranium Oxides. 2015. Thèse de doctorat. University of Bath.

[11] Khalil, Rana Muhammad Arif. Ab initio studies of the structural, dynamical and thermodynamical properties of graphitic and hydrogenated graphitic materials and their potential for hydrogen storage. 2014. Thèse de doctorat. Physics and Materials Research Centre.

[12] Thomas, Llewellyn H. The calculation of atomic fields. In : Mathematical Proceedings of the Cambridge Philosophical Society. Cambridge University Press, (1927), vol 23, no 5, p 542-548.

[13] Fermi, Enrico. Statistical method to determine some properties of atoms. Rend. Accad. Naz. Lincei, (1927), vol 6, no 602-607, p 5.

[14] Hohenberg, Pierre et Kohn, Walter. Inhomogeneous electron gas. Physical review, (1964) , vol 136, no 3B, p B864.

[15] Yin, Zhiping. Microscopic mechanisms of magnetism and superconductivity studied from first principle calculations. University of Peking, 2005

[16] W. Kohn and L. J. Sham, Self-consistent equations including exchange and correlation effects, Physical Review, (1965), vol 140, no 4A, p A1133.

[17] LI, Rui. Theoretical investigation of electronic properties of atomic clusters in their free forms and adsorbed on functionalized graphene support. 2016. Thèse de doctorat. Université de Pau et des Pays de l'Adour

[18] A. Seidl, A. G¨ orling, P. Vogl, J. A. Majewski, and M. Levy. Generalized kohn-sham schemes and the band-gap problem. Phys. Rev. B, (1996), vol 53, no 7, p 3764.

[19] PJ Stephens, FJ Devlin, CF Chabalowski, and M.J. Frisch. Ab initio calculation of vibrational absorption and circular dichroism spectra using density functional force fields. The Journal of Physical Chemistry, (1994), vol 98, no 45, p 11623–11627.

[20] Dixit, Hemant et Antwerpen, B. Partoens. Firs-principles electronic structure calculation of transparent conducting oxide materials. University antwerpen, (2012).

[21] G.B. Bachelet, D.R. Hamann, and M. Schlüter, Phys. Rev B, (1982), vol 26, p 4199.

[22] N. Troullier and J.L. Martins, Phys. Rev B, (1991), vol 43, no 3, p 1993.

[23] Steven, Bachrach, Population Analysis and Electron Densities from Quantum Mechanics, (2007), vol 5, p 171-227.

[24] D. Vanderbilt, Phys. Rev B, (1985), vol 32**,** no12, p 8412-8416.

[25] M. D. Segall, P. J. D. Lindan, M. J. Probert, , C. J. Pickard; P. J. Hasnip, S. J. Clark, M. C. Payne, J. Phys.: Condens. Matter, (2002), vol 14, p 2717-2743.

[26] AZAM, Sikander. Zásadní studie optických, termoelektrických a elektronických vlastností komplexnízh materiálů. 2016. Thèse de doctorat

[27] P.E. Blochl, Projector augmented-wave method. Physical Review B,(1994), vol 50, no 24, p 17953.

[28] Bhattacharjee, Tanushree. Towards understanding catalytic processes for the reactivity of hydrocarbons on RH surface: a quantum chemical study. 2011. Thèse de doctorat. University of Heidelberg, Germany

[29] Milan, V., Winkler, V., White, J. A., Pickard, C. J,Payne, M. C., Akhmatskaya, E. V., and R. H. Nobes, Int. Quant. Chem, (2000), vol 77, no 5, p 895

[30] Payne, M. C, Teter, M. P, Allan, D. C, Arias, T. A, and Joannopoulos, J. D, Rev. Mod. Phys, (1992), vol 64, p 1045.

[31] LENG, Biao. Simulation of Electronic and Optical Properties of Graphene. 2015. Thèse de doctorat.

[32] David Gilbert.Castep.23/03/2018. http://www.castep.org/CASTEP.

[33] Website: C.-K. Skylaris. Density Functional Theory.23/03/2018. https://www.southampton.ac.uk/assets/centresresearch/documents/compchem/DFT_L7.pdf

CHAPTER II:

Computational details and definition of calculated parameters

CHAPTER II:

Computational details and definition of calculated parameters

II.1 Delafossite structure of $CuFeO_2$:

The $CuFeO_2$ compound displays a characteristic of a delafossite group (space group number : 166; Hermann-Mauguin symbol: R $\overline{3}m$; Schoenflies symbol: D_{3D}^5). Within the delafossite structure, each Cu atom is linearly coordinated with two oxygen atoms, forming O–Cu–O parallel to the c-axis; furthermore oxygens in the O–Cu–O units are each coordinated to three Fe atoms. The delafossite $CuFeO_2$ has a Trigonal structure described by lattice parameters $a = b$, c and cell angles $\alpha = \beta = 90°$ and $\gamma = 120°$ (see figure II.1)

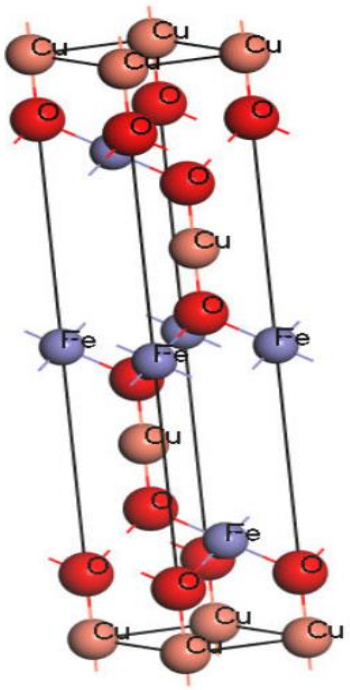

Figure II.1: The unit cell of $CuFeO_2$ delafossite compound.

By using the complementary module of visualization of structures implemented in software Materials Studio, we obtain the unit cell and the Brillouin zone with high symmetry k-points in reciprocal space for the delafossite structure of compound $CuFeO_2$ as shown in figure (II.2).

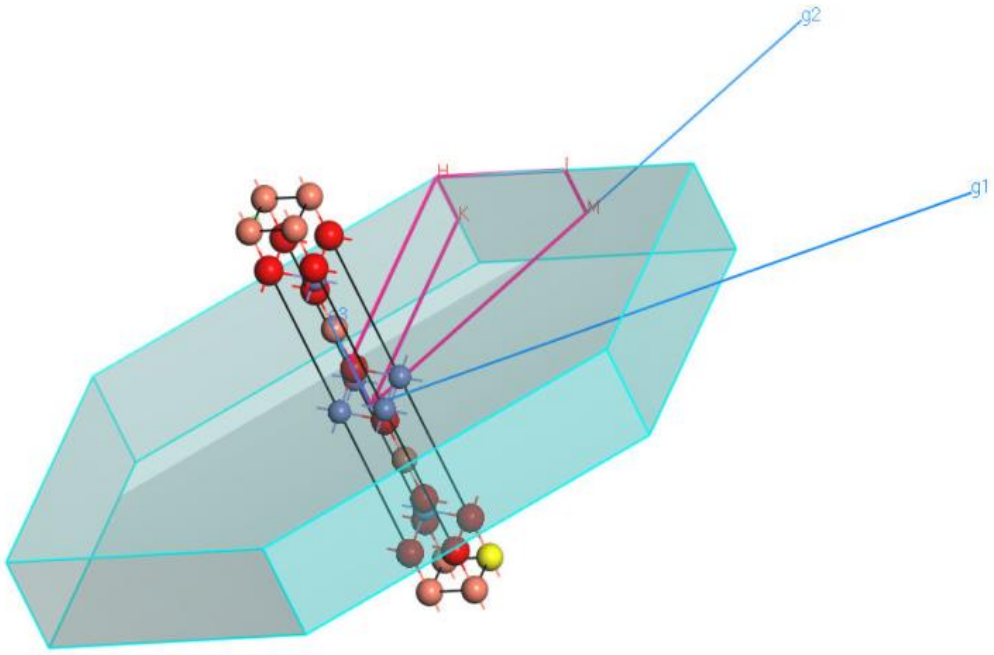

Figure II.2 : The unit cell and the Brillouin zone of the delafossite structure for **CuFeO2** compound (g_1 , g_2, $g_3$are the reciprocal lattice vectors).

II.2 Computational details:

In the present calculation we use the generalized gradient approximation of Perdew and al (GGA-PBE) [1] to evaluate of the exchange-correlation functional. Also, to describe the electron-ion interaction, we use the ultrasoft pseudo-potential of Vanderbilt extracted from the material studio library (Accelrys ©). In addition, the considered valence stats for the different atoms of the studied material are given as: O $2s^2$ $2p^4$, Cu $3d^{10}$ $4s^1$, Fe $3d^6$ $4s^2$.

The convergence criteria used here are :

- ✓ Maximal forces is : 0.01 eV/Å.
- ✓ Energy is: 5.0 10^{-6} eV/atome.
- ✓ Maximum displacement is : 5.0 10^{-4} Å.
- ✓ Maximum stress is : 0.02 GPa.

The size of the plane wave basis set is fixed by the choice of the cutoff energy: a convergence test series lead us to choose *Ecut*= 350 eV. This value has been assisted by using ultrasoft pseudo-potential which allows to reduce the cutoff energy compared to that used in the norm-conserving pseudo-potential [2].

The sampling of the first Brillouin zone has been realized by using 14 k-points which corresponds to Monkhrost-Pack points set 6×6×2. These values are chosen after a convergence test series on the desired precision.

II.3 Monkhorst and Pack special points:

In1976 Monkhorst and Pack [3], described a method consisting a set of special k-points for choose the convenient sampling of Brillouin zone. A regular grid of a k-points has been produced by the authors along the three axes in the reciprocal space.

The Monkhorst and Pack grid is defined by three integers which indicates the split number along each axe. These integers generate a series of numbers as follows:

$$u_r = {}^{(2r-q-1)}/_{2q} \qquad r = (1,2,3 \cdots q) \tag{II.1}$$

Where q is an integer that determines the number of special points in the set. Thus The Monkhorst and Pack grid is obtained from these sequences:

$$K_{prs} = u_p b_1 + u_r b_2 + u_s b_3 \tag{II.2}$$

II.4 Calculated properties:

II.4.1 The structural properties:

In a first step, we calculated the structural parameters of CuFeO2, at 0 GPa and 0 K. the results of the geometry optimization of CuFeO2 obtained by means of the CASTEP code and using plane wave ultrasoft pseudo-potential and the generalized gradient approximation (GGA) with the PBE functional.

II.4.2 Electronic properties:

In order to explore the electronic structure and the character of the atomic bonds of CuFeO2, we calculated, at zero pressure, their electronic band structure, total electronic density of states (TDOS) and partial one (PDOS), as well as the valence electronic charge distributions using the wave plane pseudo-potential and the generalized gradient approximation GGA.[2].

II.4.2.1 Band structures:

The solid state electron band structure reveals the eigenvalues associated with conduction and valence bands along specific directions in the Brillouin zone of a particular crystal structure. One of the most important reasons for calculating the electronic band structure is to determine the band gap (the energy gap), the difference between the values of the energies of the upper valence band and the lower conduction band, as this can give an idea on the potential uses for optical device applications. However, the energy gap calculated from the Kohn-Sham eigenvalues by the resolution of the Kohn-Sham equations make it possible to generate energy band structure diagrams and the electronic density of states.[2]

II.4.2.2 Density of states:

An important concept used in the analysis of the band structure is the density of states (DOS) as function of energy. There are two curves of density of states; Total Density of States (TDOS) and Partial Density of States (PDOS). For band *n*, the density of states is:

$$N_n(E) = \int \frac{dk}{4\pi^3} \delta(E - E_n(k)) \quad \text{(II.3)}$$

Where $N_n(E)$describes the dispersion of the given band and the integral is determined over the whole Brillouin zone.The total state density, N(E), is summed over all bands. The integral of N (E) from minus infinity up to Fermi level gives the total number of electrons in the unit cell.[2]

II.4.2.3 Density of charges and Mulliken population analysis:

1) Mulliken population analysis :

The Mulliken populations can serve as a means of describing the electronic distribution in an atomic or molecular system. In the CASTEP code, Mulliken population analysis is performed using a projection of plane wave states on a localized basis using a technique described by Sanchez-Portail et al. (1995) [4].The charge associated with a given atom, A, is determined by:

$$Q(A) = \sum_k w_k \sum_u \sum_v 2P_{uv}(k)2S_{uv}(k) \quad \text{(II.4)}$$

Where:

$S_{vu}(k) = \langle \phi^u(k) | \phi^v(k) \rangle$: is the overlap matrix (II.5)

$P_{uv}(k) = \langle \phi^u(k) | \rho(k) | \phi^v(k) \rangle$: is the density matrix (II.6)

$W_{\alpha u}(k) = \langle \psi^\alpha(k) | \phi^u(k) \rangle \langle \phi^\alpha(k) | \psi^\alpha(k) \rangle$: is the band weight α on the orbital$u$. (II.7)

2) Electronic density of charges :

The electronic density of charges distribution is an important property of solids in that it provides a good description of the chemical properties [5]. The electronic density of charges is given by the following expression:

$$\rho(\vec{r}) = \frac{(2\pi)^3}{\Omega} \int d\vec{k} \sum_i f_{ik} [\rho_i(k)]^2 \quad \text{(II.8)}$$

The sum is done on the occupied orbitals and the integral extends over the first Brillioun zone.

II.4.3 Optical properties:

In solids, optical properties provide a unique opportunity for the experimental study of band structures, excitations, defects, impurity levels, magnetic excitations and lattice vibration [6].

II.4.3.1 Dielectric function:

The study of the optical functions helps to give a better understanding of the electronic structure. One of such functions is the complex dielectric function [7];

$$\varepsilon(\omega) = \varepsilon_1(\omega) + i\varepsilon_2(\omega) \quad \text{(II.9)}$$

Where $\varepsilon_2(\omega)$ is the imaginary part and is given by [8] :

$$\varepsilon_2(\omega) = \frac{8}{3\pi\omega^2} \sum_{nn'} \int \left| P_{nn'}(k) \right|^2 \frac{ds_k}{\nabla\omega_{nn'}(k)} \quad \text{(II.10)}$$

$P_{nn'}(k)$ Are the elements of the dipolar matrix between an initial state $|nk\rangle$ and the final state n'k, their eigen energies are $E_n(k)$ and $E_{n'}(k)$, respectively

$$\omega_{nn'}(k) = E_n(k) - E_{n'}(k) \quad \text{(II.11)}$$

S_k An energy-efficient surface expressed by :

$$S_k = \{k, \omega_{nn'}(k) = \omega\} \quad \text{(II.12)}$$

Thus The real part $\varepsilon_1(\omega)$ of the frequency-dependent dielectric function can be derived from the imaginary part using the Kramers Kronig relation [9]:

$$\varepsilon_1(\omega) = 1 + \frac{2}{\pi} P \int_0^{\infty} \frac{\omega' \varepsilon_2(\omega')}{\omega'^2 - \omega^2} d\omega' \quad \text{(II.13)}$$

P : is the principal value of the integral given as.

$$P = \lim_{a\to 0} \int_{-\infty}^{\omega - a} \frac{\varepsilon(\omega')}{\omega' - \omega} d\omega' + \lim_{a\to 0} \int_{\omega - a}^{+\infty} \frac{\varepsilon(\omega')}{\omega' - \omega} d\omega' \quad \text{(II.14)}$$

By using the above expressions we can calculate important optical functions such as the refractive index $n(\omega)$ optical conductivity, reflectivity function, electron energy loss spectra and absorption coefficient [7] :

- Refractive index: becomes complex; the real part is generally the refractive index n and the imaginary part is called the extinction coefficient$k$. They can be expressed as:

  1. $n(\omega) = \frac{1}{\sqrt{2}} \left[\{\varepsilon_1(\omega)^2 + \varepsilon_2(\omega)^2\}^{1/2} + \varepsilon_1(\omega) \right]^{1/2}$ (II.15)
  2. $k(\omega) = \frac{1}{\sqrt{2}} \left[\{\varepsilon_1(\omega)^2 + \varepsilon_2(\omega)^2\}^{1/2} - \varepsilon_1(\omega) \right]^{1/2}$ (II.16)

- Optical conductivity function σ : $\sigma(\omega) = \frac{2W_{cv}\hbar\omega}{E}$ (II.17)
  Where W_{cv} is the transition probability per unit time.

- Reflectivity : $R(\omega) = \left|\frac{\tilde{n}-1}{\tilde{n}+1}\right| = \frac{(n-1)^2 + k^2}{(n-1)^2 + k^2}$ (II.18)
- Absorption coefficient : $a(\omega) = \frac{4\pi k(\omega)}{\lambda}$ (II.19)
- The optical loss : $L(\omega) = -Im\left(\frac{1}{\varepsilon(\omega)}\right) = \frac{\varepsilon_2(\omega)}{\varepsilon^2{}_1(\omega) + \varepsilon^2{}_2(\omega)}$ (II.20)

II.4.4 Elastic properties:

The elastic constants of solids provide a link between the mechanical and dynamical behaviors of crystals, and give important information concerning the nature of the forces operating in solids [2]. The crystal returns to its original form once the constraint is removed, in the elastic region where the constraint is less than a certain limit value and the deformation will be temporary. The deformation on a solid is then linearly proportional to the magnitude of the applied stress, which is associated with slight variations in interatomic distances, and then considerable variations in cohesion energy.

Elasticity is a general property of solids that was stated by Hooke in 1660 and generalized after that by Cauchy. This law proposed to express the constraint tensor σ (the cause) as a linear function of deformation tensor one ε (the effect) as (Hook's law):

$$\boldsymbol{\sigma_i = c_{ij}\varepsilon_k} \tag{II.21}$$

Or

$$\boldsymbol{\varepsilon_i = s_{ij}\sigma_j} \tag{II.22}$$

Where i, j=1,..6 are Voigt notation, and C_{ij} and S_{ij} elements are the symmetric elasticity (stiffness) tensor and compliance (flexibility) tensor, respectively.

By taking into account the symmetry of structure (Trigonal system with space group $R\bar{3}m$), the number of the independent parameters is 6. Also, the symmetry of crystal reduce the number of independent parameters; a totally anisotropic material, which presents no symmetry operation, has only two independent elastic constants C_{11} and C_{12}.

According to J.F Nye [10], the elastic constants matrix takes the following form:

$$\begin{pmatrix} C_{11} & C_{12} & C_{13} & C_{14} & 0 & 0 \\ 0 & C_{11} & C_{13} & -C_{14} & 0 & 0 \\ 0 & 0 & C_{33} & 0 & 0 & 0 \\ 0 & 0 & 0 & C_{44} & 0 & 0 \\ 0 & 0 & 0 & 0 & C_{44} & C_{14} \\ 0 & 0 & 0 & 0 & 0 & \frac{1}{2}(C_{11} - C_{12}) \end{pmatrix} \tag{II.23}$$

$\boldsymbol{C_{ij}}$ Elastic constants are often used to characterize the elastic behavior of single crystals **(**anisotropic parameters). These parameters can be determined efficiently from ab initio calculations.

The isotropy of material results from an average of anisotropic properties of many mono crystals and the elastic properties do not depend on the orientation within the material. The Young's modulus, characterizing uniaxial rigidity of a solid or the solid resistance to the uniaxial deformation, is given by:

$$E_{ii} = \sigma_{ii}/\varepsilon_{ii} \tag{II.24}$$

The shrinking along the axis perpendicular to the direction of the stress is characterized by the Poisson's coefficient, given as :

$$\eta_{ij} = -\varepsilon_{ii}/\varepsilon_{jj} \quad \text{(II.25)}$$

It is worth noting that the elastic behavior of a polycrystalline system is described only by two elastic constants; bulk modulus B and shear modulus G, the two Lamé's constants (λ and μ) or Young's modulus (or rigidity) E and Poisson's ratio η [2]. The shear modulus G (form changing under constant volume) and the bulk modulus B (volume changing under constant form) are expressed as:

$$\tau = G\gamma \qquad B = V\frac{d^2U}{dV^2} \quad \text{(II.26)}$$

U: is the energy of unit cell in volume V and $\gamma = 2\varepsilon_d$ is the shear deformation.

A set of monocrystalline grains, each has its own crystalline orientation with differently response to the applied stress, compose the polycrystalline material. In order to calculate the elastic properties of polycrystalline structure, various methods, based on averaging the different responses, have been proposed.

Voigt [11], proposed that the deformation is assumed to be constant throughout the polycrystalline and equals to the macroscopic deformation applied on the sample. This returns to take an average on the elastic modulus C_{ij} over the entire space of orientations. Then, the compressibility modulus and shear's modulus are given by:

$$B_V = \frac{1}{9}[2(C_{11}+C_{12})+C_{33}+4C_{13}],\ G_V = \frac{1}{5}\left(G_{eff}^V + 2\mu_1 + 2\mu_2\right) \quad \text{(II.27)}$$

With $G_{eff}^V = \frac{1}{3}(C_{11}+C_{33}-2C_{13}-C_{66})$, $G_{eff}^r = \frac{(C_{11}+C_{12})C_{33}-2C_{13}^2}{6B_V}$, $\mu_1 = \frac{1}{2}\{C_{44}+C_{66}+[(C_{44}-C_{66})^2+4C_{14}^2]^{1/2}\}$ and $\mu_2 = \frac{1}{2}\{C_{44}+C_{66}-[(C_{44}-C_{66})^2+4C_{14}^2]^{1/2}\}$.

Also, Reuss [12], proposed that the constraint is assumed to be constant throughout the polycrystalline and equals to the microscopic constraint. Then, the coefficients *B* and *G* are written as:

$$B_R = \frac{(C_{11}+C_{12})C_{33}-2C_{13}^2}{6G_{eff}^r}, \qquad G_R = \left[\frac{1}{5}\left(\frac{1}{G_{eff}^r}+\frac{2}{\mu_1}+\frac{2}{\mu_2}\right)\right]^{-1} \quad \text{(II.28)}$$

Then, the elasticity modulus *B* and *G* are approximated by Hill's average [13], and given as follows :

$$B^{Hill} = (B^{Voigt} + B^{Reuss})/2\,, \quad G^{Hill} = (G^{Voigt} + G^{Reuss})/2 \tag{II.29}$$

Shear's modulus, Young's modulus, Poisson's coefficient and Lamé's constants, are written, respectively, as:

$$G = \frac{1}{2(S_{11}-S_{12})} = \frac{1}{S_4},\ E = \frac{1}{S_{11}},\ \eta = -\frac{S_{12}}{S_{11}},\ u = C_{44} = \frac{1}{2}(C_{11}-C_{12}) = \frac{1}{S_{44}} = G,\ \lambda = C_{12} \tag{II.30}$$

This is done taking into account that for an isotropic system the elasticity matrix and suppleness constants are reduced as:

$$\begin{bmatrix} C_{11} & C_{12} & C_{12} & 0 & 0 & 0 \\ . & C_{11} & C_{12} & 0 & 0 & 0 \\ . & . & C_{11} & 0 & 0 & 0 \\ . & . & . & \frac{C_{11}-C_{12}}{2} & 0 & 0 \\ . & . & . & . & \frac{C_{11}-C_{12}}{2} & 0 \\ . & . & . & . & . & \frac{C_{11}-C_{12}}{2} \end{bmatrix} \tag{II.31}$$

$$\begin{bmatrix} S_{11} & S_{12} & S_{12} & 0 & 0 & 0 \\ . & S_{11} & S_{12} & 0 & 0 & 0 \\ . & . & S_{11} & 0 & 0 & 0 \\ . & . & . & 2(S_{11}-S_{12}) & 0 & 0 \\ . & . & . & . & 2(S_{11}-S_{12}) & 0 \\ . & . & . & . & . & 2(S_{11}-S_{12}) \end{bmatrix} \tag{II.32}$$

REFERENCES:

[1] Perdew, J.P.; Burke, K.; Ernzerhof, M, Generalized Gradient Approximation Made Simple, *Phys. Rev. Le*, (1996), vol **77**, p 3865-3868.

[2] Kh. Haddadi. Etude des propriétés structurales, élastiques et électroniques des composés antiperovskites de type XNCa3.2013.Thèse Doctorat ès Science. Univ. Ferhat Abbas de Sétif

[3**]** H. J. Monkhorst and J. D. Pack. Phys. Rev B, (1976), vol 13, no 12, p 5188.

[4] R. S. Mulliken, J. Chem. Phys., (1955), vol 23, no 10, p 1833

[5] CHERRAD, DJELLAL. Étude Ab initio des propriétés structurales, élastiques, électroniques et optiques des perovskites CaXO3 (X= Sn et Hf) dans la phase cubique et orthorhombique. 2012. Thèse de doctorat. Université Ferhat Abbas de Sétif 1.

[6] M. Dresselhaus and M. Dresselhaus, \Optical properties of solids," Proc. Of Int. School of Phys.Enrico Fermi, (1966), p 243.

[7] C. Amrosch-Draxl, J.O.Sofo Linear optical properties of solids within the full-potential linearized augmented planewave method. Omput. Phys. Commun, (2006), Vol 175, no 1, p 1-14.

[8] M.A. Khan, A. Kasphyop, A. K. Solanki, T. Nautiyal, and S. auluck, Phys. Rev B, (1993), vol 48, no 23 **,** p 16974.

[9] F. Wooten, Optical Properties of Solids. Academic Press, New York and London. (1972).

[10] coefficients of the matrices of the stresses and deformation according to J.F Nye

[11] W. Voigt, Lehrburch der Kristallphysik. Leipzig: Teubner,(1928), p 716-761.

[12] A. Reuss, Angew Z. Math. Mech, (1929) ,Vol 9, p49.

[13] R. Hill, Proc. Phys. Soc. London, (1952), vol 65, p396.

CHAPTER III :

Results & discussion

CHAPTER III:

Results & discussion

III.1 Structural properties:

Table (III-1) summarizes the lattice parameter values and *interatomic distance d* of studied $CuFeO_2$ compound in Trigonal phase $R\bar{3}m$, compared with some experimental results [1] thus available other theoretical [1.2] Calculations are made using the GGA approximation.

Table (III.1) : Lattice parameters *a=b, c* and interatomic distance d.

Parameter	Present values	Theoretical	Experimental
a=b (A°)	2,873	2.976 [1] 3.0344 [2]	3.035 [1]
c(A°)	17,217	17.0 [1] 17.158[2]	17.167 [1]
d_{Cu-O} (A°)	1.866		
d_{Fe-O} (A°)	1.938		

It is well known that in general the GGA overestimates the structural parameters, whereas the LDA underestimates them. From reported values in the above table it's clear that, the relative deviation between the present values and the theoretical (experimental) ones are very little: for the lattice parameter **a = b** (**c**), it is ranging from 3.58% to 5.61% (0.34% to 1.26%) compared with theoretical results, whereas it is of the order of 5.64% (0.29%) relative to other experimental results.

III.2 Electronic properties:

Knowledge of the diagrams of the structure of the energy bands is indispensable, if the semiconductor in question is incorporated in the family of materials considered for electronic applications. These diagrams show how the electronic energies depend on the wave vector k, along a high symmetry direction in the first Brillouin zone and can be used to explore the electronic and optical properties of semiconductors.

III.2.1 Electronic band structure:

We have calculated the band structure diagram of $CuFeO_2$ using the GGA approximation. The band structures are given in Figure (III.1) for delafossite $CuFeO_2$ compound along the six lines of high symmetry including the points G, A, H, K, L and M, in the reducible zone of Brillouin.

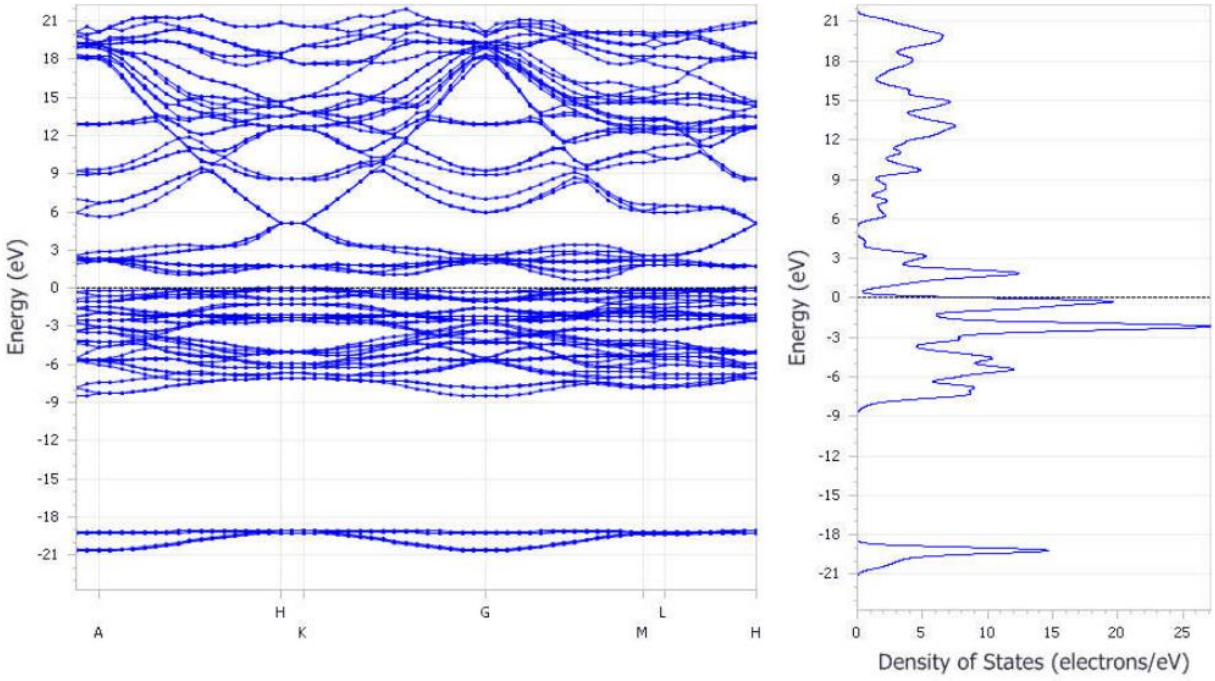

Figure (III.1): Band structures and total density of states (TDOS) of CuFeO2.

The Fermi level E_F is chosen to be 0 eV (dotted horizontal streak) and it's located at the maximum of the valence band, we can observe that the TDOS at the edges of the band gap decreases.

III.2.2 Density of states:

The total (TDOS) and partial (PDOS) density of states obtained by the GGA of delafossite $CuFeO_2$ are shown in Figure (III.2), We have found that the total state density (TDOS) of our compounds can be divided into two parts separated by the fundamental gap

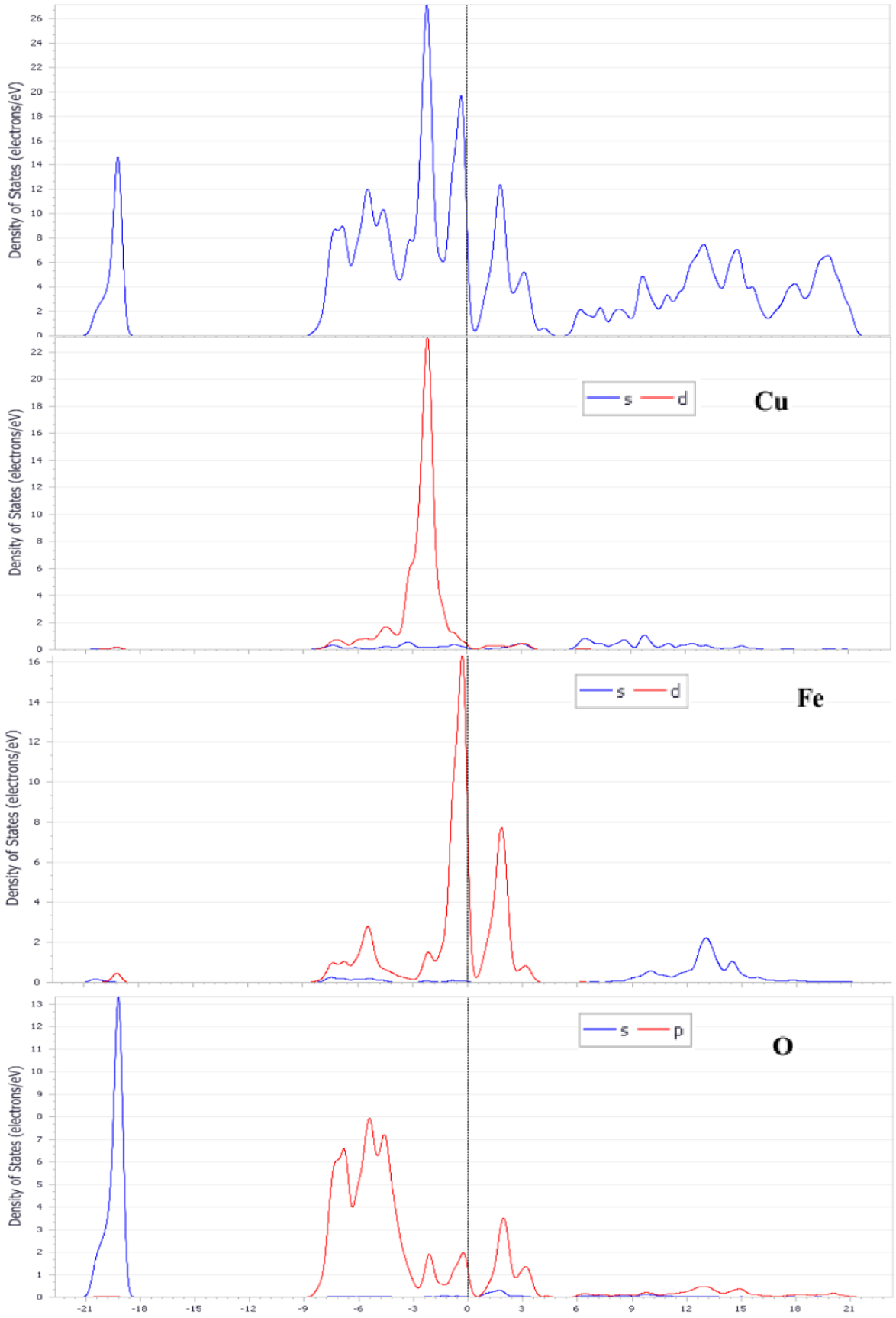

Figure (III.2): The total (TDOS) and partial (PDOS) density of states of $CuFeO_2$.

For CuFeO2, below the Fermi level, the energy range between -9 to 0 eV is due to the hybridization of the states of Fe d and Cu d with some states of O p. The minimum of the conduction band located at 2 eV originates from the hybridization of the states of Fe d with some states of oxygen O p. The structure located in the range of energy between 6 to 21 eV is dominated mainly by the electrons states of Fe s and Cu s with some mixture from the state Op.

III.2.2 Electronic energy gap:

By definition, the fundamental energy gap of an insulator material incorporated in the family of semiconductors or that of dielectrics is the difference between the maximum of the valence band and the minimum of the conduction band [3]. The band structure shown in Figure (III.1) allows the calculation of the values of the direct and indirect gaps in Tables (III.2). These gap values are very important for the study of the optical transitions that follow.

For ideal $CuFeO_2$ Figure (III.1), we find that the top of the conduction band (CB) is located at the point of symmetry H, and the bottom of the valence band (VB) is located at the point along GM high symmetry axis. Therefore, this compound has an indirect band gap of about 0.630.

Table (III.2): Energy band gaps for **$CuFeO_2$** with the available experimental and theoretical values.

Energy band gap	**Present work**	**Theoretical**	**Experimental**
Indirect (H-F) F is located along GM high symmetry axis.	0.630		3.69 [4]
Direct (G-G)	2.368		

Theoretically, the band gap of $CuFeO_2$ is due to the conduction band of Fe 3d+O 2p states and the valence band of Cu 3d + O 2p states.[5.6]

Also from the figure (III.1) we can evaluate The values of the valence band (BV) and The conduction band (BC) along high symmetry points (Tables III.3).

Direct		Indirect									
G-G	2,368	G-A	2,241	A-H	2,113	H-K	1,727	K-M	1,849	M-L	1,906
A-A	2,351	G-H	2,003	A-K	2,113	H-M	1,852	K-L	1,864	L-G	2,139
H-H	1,727	G-K	2,003	A-M	2,238	H-L	1,867	M-G	2,131	L-A	2,012
K-K	1,724	G-M	2,128	A-L	2,253	K-G	2,089	M-A	2,004	L-H	1,774
M-M	1,891	G-L	2,143	H-G	2,092	K-A	1,962	M-H	1,766	L-K	1,774
L-L	1,914	A-G	2,4783	H-A	1,9656	K-H	1,724	M-K	1,766	L-M	1,899

Table (III.3): Calculated indirect and direct energy band gaps (eV) of $CuFeO_2$.

We believe that all the values we have found from the diagrams of the band structure are underestimated, therefore lower than the real ones. This can be interpreted by the fact that at ambient temperature the vibrations of the structure are not taken into consideration. Moreover, the resolution of the Schrödinger equation is done by using an exact wave function, without taking into account the spin-orbit interaction.

In addition, the LDA and GGA approximations generally underestimate the energy gaps. This is mainly comes back because they have simple forms that are not flexible enough to get the exact form of exchange and correlation potential [7].

III.2.3 Mulliken's population analysis:

As we denoted in the previous chapter, the ionic character of a material may be related to the charge transfer between the cations and the anions constituting it. In order to explore the chemical bonds of $CuFeO_2$, we calculated the transferred charge between cations and anions based on the Mulliken population analysis.

Species	ion	S(e)	P(e)	D(e)	total	Charge
O	1-6	1.84	4.74	0.0	6.58	-0.58
Fe	1-3	0.28	0.3	6.48	7.07	0.93
Cu	1-3	0.6	0.52	9.65	10.77	0.23

Table (III.4): Calculated Mulliken partial, total and transferred charges.

From the table we can conclude the following:

- ✓ Each O atom receives 0.58 e from the total charge transferred by the tow other atoms Cu (0.23e) and Fe (0.93e).
- ✓ The formal valence states of the considered material:$Cu^{+2}Fe^{+2}O^{-2}$.
- ✓ Effective valence states predicted through the calculations results : $Cu^{+0.23}\ Fe^{+0.93}O^{-0.58}{}_2$.

- ✓ The difference of the electronegativity of the constituent atoms of **$CuFeO_2$** (3.44: O, 1.9; Cu and 1.83; Fe). Is the main reason of this transfer of charge.

The ionic character of a material can be estimated from the effective ionic valence, which is defined by the difference between the formal ionic charge and the Mulliken charge. A value of zero indicates a purely ionic bond, while values greater than zero indicate increasing levels of covalency [8]. Hence, the effective ionic valence of Cu is 1.77, and Fe is 1.07.

III.2.4 Charge density of valence electrons:

The charge density distribution from (110) plane of $CuFeO_2$ is presented in figure (III.3). This distribution allows us to explore the nature of chemical bonding between atoms. We observe that there is an interaction between the charges of Fe and O on the one hand and between those of Cu and O on the other hand. The density of electronic charges is slightly asymmetric for both bonds. So, the large transfer of charges from the cation to the anion indicates that the anion (O^{-2}) has a higher electronegativity(3.44)[9] than that of the cation (Cu^{+2} (1.9) [9] and Fe^{+2} (1.83) [9]). The high ionic valence of Cu (1.77 e) compared to Fe (1.07 e) indicates that the Cu-O bond is much more covalent than the Fe-O bond.

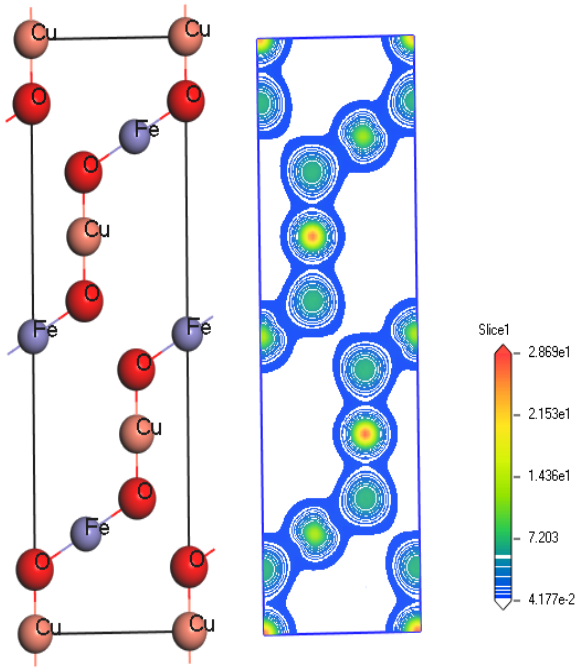

Figure (III.3): Charge density distribution (e/A^3) from (110) plane of $CuFeO_2$.

III.3 Optical properties:

III.3.1 Dielectric function:

One of the most important optical characteristic to describe the behavior of semiconductors undergoes to the effect of external light excitation, is the complex dielectric function. The real and imaginary parts of complex dielectric function $\varepsilon(\omega)$ for semiconductor compound $CuFeO_2$ are shown in figure (III.4):

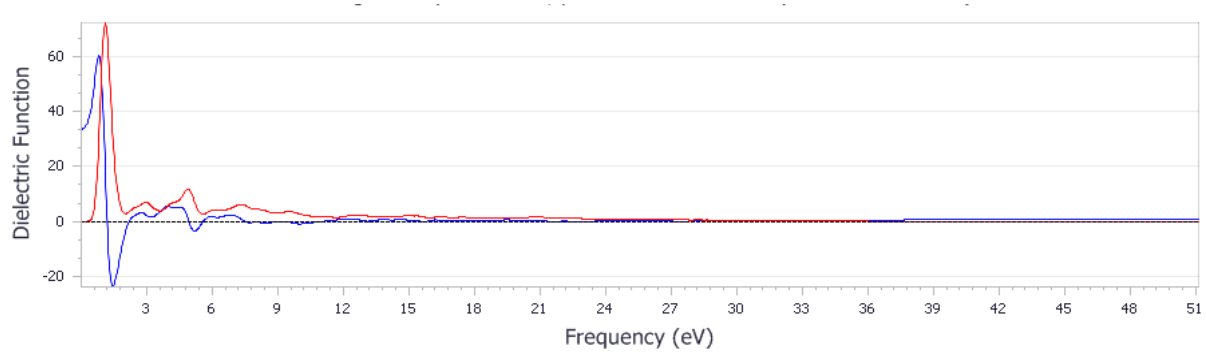

Figure (III.4): Dielectric function, the real part $\varepsilon_1(\omega)$ (in blue) and the imaginary part $\varepsilon_2(\omega)$ (in red), of **$CuFeO_2$.**

Where it have been calculated under condition of illumination light less than or equal to 50 eV. The static dielectric constant $\varepsilon_1(0)$ obtained at zero pressure was about 35.4. The observed peaks are mainly produced from the electronic transition of the valence band to the states forming the conduction band's orbitals. Moreover, the beginning of the energetic spectrum $\varepsilon_2(\omega)$ is corresponding to a transition close to the indirect energy gap about 0.6 eV.

III.3.2 Optical absorption:

Figure (III.5) shows the optical absorption spectra of $CuFeO_2$. The absorption peak is observed at 22 eV. This absorption peak was primarily attributed to the charge-transfer excitation from the valence band to the conduction band [5, 10]. The extracted direct optical band gaps of $CuFeO_2$ are in the range 3.25–4.45 eV. [11.12]. For our compound the absorption start in about 0,6 eV corresponds the indirect band gap (0,63 eV), known as fundamental absorption threshold. This originates from transitions of Fe 3d and Cu 3d electrons of the valence band to the O 2p empty orbital dominating the deep conduction band.

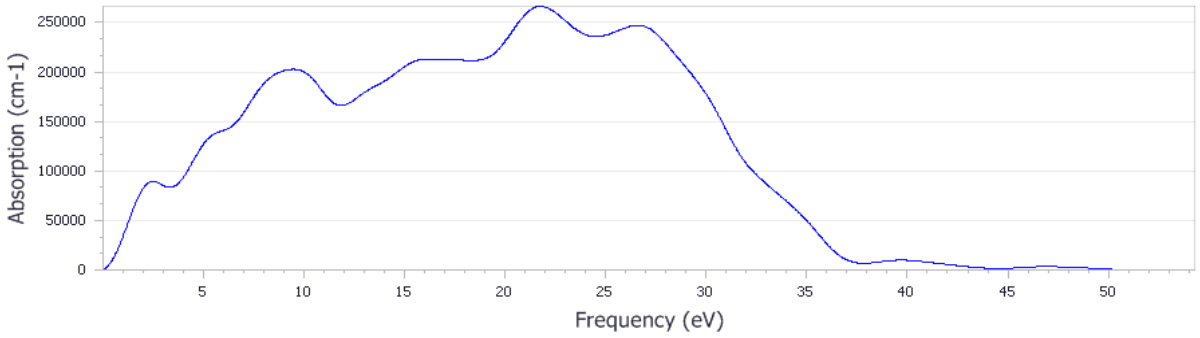

Figure (III.5): Linear absorption $\alpha(\omega)$ spectrum of $CuFeO_2$ compound.

III.3.3 Refractive index:

One of the most important optical constants is the refractive index, which in general depends on the wavelength of the electromagnetic wave, by a ratio called the dispersion. The case where an electromagnetic wave can lose its energy during its propagation, the refractive

index becomes complex. The real part is usually the index of refraction n, and the imaginary part is called the extinction coefficient k.

Here, we study the complex refractive index among optical properties for the $CuFeO_2$. In Fig (III.6), both the real and the imaginary parts of complex refractive index are illustrated. It is clearly seen that in a high-energy region, where the frequency of photons is corresponding to the energy larger than 5eV, the values of the real part are very small, while the values of the imaginary part change very little. Also, the static refractive index n (0) is found to be 5.5. Moreover, the refractive index spectrum increases with the photon energy evolution in the visible range of the solar spectrum.

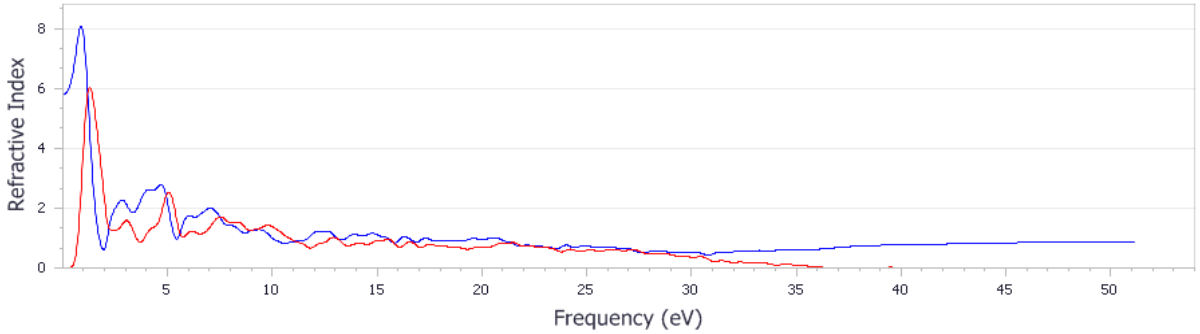

Figure (III.6): The refractive index $n(\omega)$ (in bleu) and the extinction $k(\omega)$ (in red) spectrums of **$CuFeO_2$.**

III.3.4 Reflectivity:

For the reflectivity curve shown in Fig (III.7) the first or strongest absorption peak takes place around 1.8 eV. However, at high-energy region, where photon energy is larger than about 36eV, the reflection is very weak and slowly goes to zero with increasing photon energy.

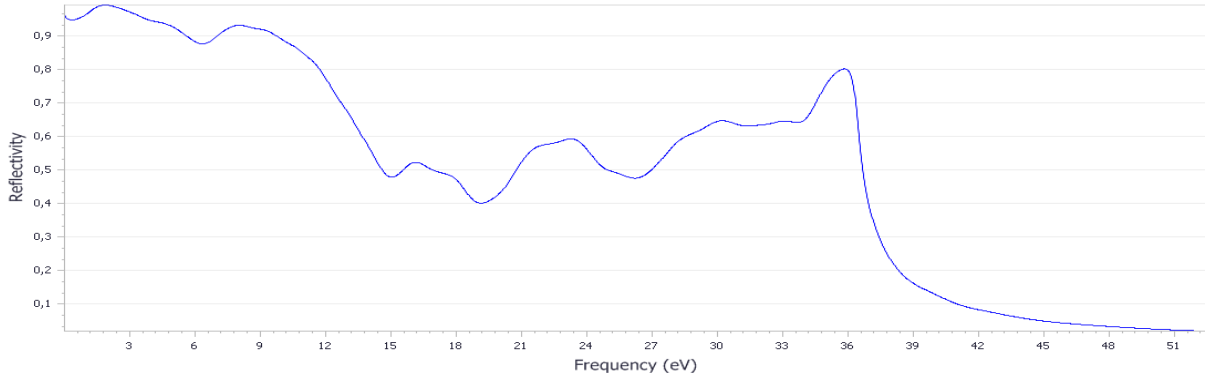

Figure (III.7): Reflectivity $R(\omega)$ of $CuFeO_2$ compound.

III.3.5 The optical loss:

The electron energy-loss spectrum $L(\omega)$ is shown in Fig (III.8). $L(\omega)$ Describes the energy loss of a fast electron traversing in a material. From Fig (III.8), we can see that there is prominent peak in $L(\omega)$ spectra which represent the characteristic associated with the plasma resonance is located at 36 eV. Also, the most pronounced peak of L (ω) corresponds to the beginning of the abrupt decrease of the intensity of R (ω).

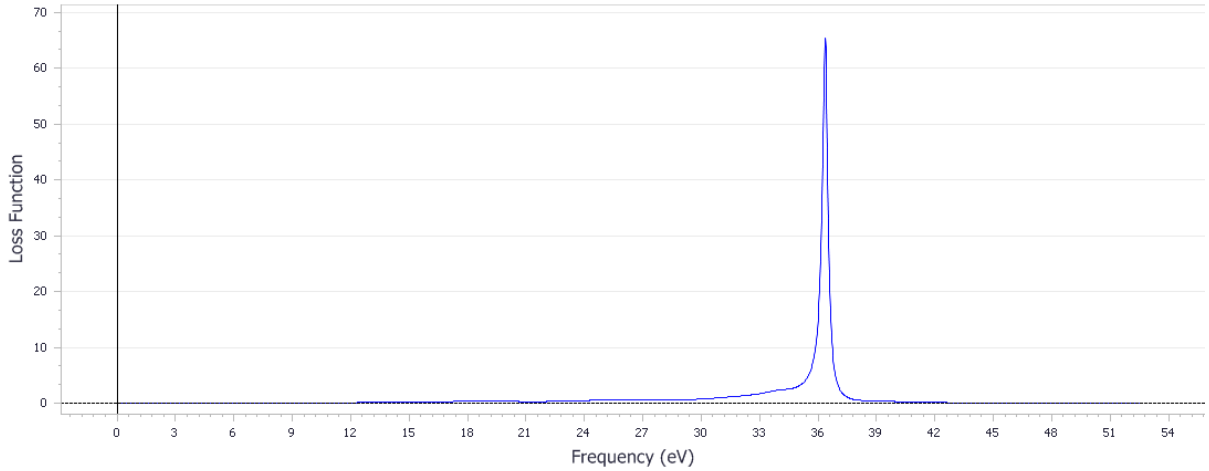

Figure (III.8): Loss function $L(\omega)$ of $CuFeO_2$.

III.4 Elastic properties:

The elasticity of the solids is closely related to the mechanical and dynamic behavior of the crystals giving important information concerning the structural stability and the nature of the forces existing in the solids.

III.4.1 Monocrystalline state:

The elastic behavior of a Tetragonal monocrystalline system is completely characterized by six independent elastic constants C_{11},C_{12} ,C_{13} ,C_{14} ,C_{33} and C_{44}. The elastic constant C_{ii} reflects the resistance of the crystal to unidirectional compression along the main directions, The constant C_{44} represents the resistance to shear stress applied , The constant C_{12} has no simple physical meaning but its combination with other constants provides additional information about the elastic behavior, for example the C_{66} Tetragonal shear constant, which exhibits shear strain resistance across the plane (110), can be estimated by combining C_{12} and C_{11} via the relation: $C_{66} = (C_{11} - C_{12})/2$.

So to evaluate the elastic properties of $CuFeO_2$ compound we calculated anisotropic values of elastic Stiffness and Compliance constants, Young's modulus E, bulk modulus B, Poisson's ratio under zero pressure condition. All the calculated results are registered in the Table (III.5).

***Table*(*III*. 5):** Elastic constantsC_{ij}, Young's modulus E_X,E_Y, E_Z, bulk modulus *B*, Poisson's ratio E_{XY}, E_{YX}, E_{ZX},E_{XZ}, E_{YZ} and E_{ZY}.

Parameter	**Values**	**Parameter**	**Values**
C_{11} C_{12}	154.93 145.52	Ey	-1.81974
C_{13} C_{14}	146.52 16.00	Ez	257.20
C_{33} C_{44}	400.12 49.65	Exy Exz (GPa)	1.0094 -0.0035
B (GPa)	150.17	Eyx Eyz(GPa)	1.0094 -0.0035
Ex	-1.81974	Ezx Ezy (GPa)	0.4877 0.4877

The material studied is characterized by a large C_{ii} value compared to C_{12}, C_{14} and C_{44}, meaning they are more resistant to unidirectional compression than to shear deformations. Also, the material is more resistant along c-axis.

In addition, the consideration of the mechanical stability of the crystal lattice was originally formulated by Born and Huang [13-14] who showed that by developing the internal energy of a crystal in a series of power constraints, it is possible to obtain stability criteria in terms of conditions on the elastic constants, while considering the positive energy. The condition of dynamic or mechanical stability of a material implies that the energy variation under any small deformation is positive. This condition can be formulated in terms of elastic constants C_{ij}[14].

For a Tetragonal system, the six independent elastic constants are required to satisfy the following conditions [15]:

$$\begin{cases} C_{11} > |C_{12}| \\ C_{44} > 0 \\ C^2{}_{13} < \frac{1}{2} C_{33}(C_{11} + C_{12}) \\ C^2{}_{14} < \frac{1}{2} C_{44}(C_{11} - C_{12}) = C_{44}C_{66} \end{cases} \quad \text{(III.1)}$$

In fact any mechanical strain must increase the total mechanical energy of a system at equilibrium. Concerning this criterion, it seems to be necessary to emphasize that in crystals belonging to the 3m classe, the Born criterion gives rise to only two conditions [16]:

$$\begin{aligned} B_1 &= (C_{11} + C_{12})C_{33} = 2C^2{}_{13} \\ &= 2\big((C_{11} - C_{66})C_{33} - C^2{}_{13}\big) > 0 \end{aligned} \quad \text{(III.2)}$$

And

$$\begin{aligned} B_2 &= (C_{11} - C_{12})C_{44} - 2C^2{}_{14} \\ &= 2(C_{66}C_{44} - C^2{}_{14}) > 0 \end{aligned} \quad \text{(III.3)}$$

The values found for the C_{ij} delafossite obey these conditions, thus indicating the mechanical stability of the Tetragonal structure for the $CuFeO_2$ material.

III.4.2 Polycrystalline state:

The polycrystalline elastic constants were calculated from monocrystalline elasticity modulus by transforming them to a macroscopic quantity using methods allowing the

calculation of average values based on a static mechanics. In this study, we used three methods (Voigt, Reuss and Hill; see previous chapter) to compute the values of the isotropic modulus.

Isotropic elastic modulus, compressibility's modulus *B*, Lamé coefficient λ et μ (shear module), Young modulus and Poisson ratio under P=0 GPa, are gathered in Table (III.6).

Parameter	Voigt	Reuss	Hill
Bulk modulus	176.34934	150.17425	163.26180
Shear modulus	38.89507	-1.03699	18.92904
Lame lambda	150.41929	150.86558	150.64244
Young modulus	108.69414	-3.11816	54.67410
Poisson ratio	0.39727	0.50346	0.44419

***Table*(*III*. 6)**: Elastic modulus for polycrystalline material (GPa).

The Poisson's ratio η, which measures the stability of the crystal against shearing, formally takes values between -1 and 0.5, which correspond, respectively, to the lower limit where the material does not change its shape and to the upper limit when the volume does not change. The value of η which equal to 0.5, calculated by Reuss method for the $CeFeO_2$ indicates that the volume does not change.

To determine if a material is fragile (brittle) or malleable (ductile), Pugh [17] has proposed the empirical relation $\left({}^{B}/_{G} = 1.75\right)$ connecting the modulus of compressibility B to the shear modulus. For ${}^{B}/_{G} > 1.75$, the material is malleable, otherwise for ${}^{B}/_{G} < 1.75$, the material is fragile. The values of the ratio ${}^{B}/_{G} > 1.75$ for our compound ($CuFeO_2$). Thus it should be classified as ductile material.

REFERENCES:

[1] F. Ye, Y. Ren, Q. Huang, J. A. Fernandez-Baca, P. Dai, J. W. Lynn, and T.Kimura, Phys. Rev B,(2006), vol 73, no22, p 220404.

[2] LALANNE, Maëva, BARNABÉ, Antoine, MATHIEU, Florence, et al. Synthesis and Thermostructural Studies of a $CuFe_{1-x}Cr_xO_2$ Delafossite Solid Solution with $0 \leq x \leq 1$. Inorganic chemistry,(2009), vol 48, no 13, p 6065.

[3] C. Kittel, Physique de l'état solide, Cours et Problèmes, 7ème édition, éditions Dunod (1996).

[4] Naka-in, Lerdkead, et al. Effects of Ge substitution on the structural and physical properties of CuFeO2 delafossite oxide, Japanese Journal of Applied Physics,(2015), vol 54, no 4S, p 04DH10.

[5] H. Hiraga, T. Makino, T. Fukumuura, H. Weng, and M. Kawasaki, Phys.Rev B,(2011), vol 84, no 4, p 041411.

[6] D. Yoo, I. Kim, S. Kim, C. H. Hahn, C. Lee, and S. Cho, Appl. Surf. Sci,(2007) Vol 253, no 8, p 3888.

[7] M. Segall, M. Probert, C. Pickard, P. HasnipS. Clark, K. Refson, M. Payne, CASTEP version 3.2 Ab Initio Total Energy Program. (2004).

[8] M.D. Segall, R. Shah, C.J. Pickard, and M.C. Payne, Phys. Rev B, (1996), vol 54, no 23, p 16317.

[9] Site web: https://www.lenntech.fr/francais/data-perio/electronegativite.htm

[10] Y. Li, W. Bo, M. Zhong, Y. Hu, M. Zhu, H. Zhang, Y. Li, and H. Zhao,Phys. Status Solidi C,(2013), vol 10, p 1276.

[11] F. A. Benko and F. P. Koffyberg, J. Phys. Chem. Solids, (1987), vol 48, no5, (1987), p 431.

[12] M. M. Moharam, M. M. Rashad, E. M. Elsayed, and R. M. Abou-Shahba, J. Mater. Sci.Mater. Electron,(2014), Vol 25, no 4 ,p 1798.

[13] C. Zener, Elasticity and Anelasticity of Metals, University of Chicago Press, Chicago, (1948).

[14] W. Voigt, Lehrburch der Kristallphysik. Leipzig: Teubner; (1928), p 716.

[15] Mouhat, Félix et Coudert, François-Xavier. Necessary and sufficient elastic stability conditions in various crystal systems. Physical Review B, (2014), vol 90, no 22, p 224104.

[16] M. Carpenter and E. Salje, Eur. J. Mineral, (1998), vol 10, p 693

[17] S.F. Pugh, Phil. Mag,(1954), vol 45, no 367, p 823.

General conclusion

General conclusion:

The plane wave ultrasoft pseudo-potential methods and the generalized gradient approximation (GGA) have been used to describe the exchange-correlation energy within the density-functional theory as implemented in the CASTEP code.

The structural, optical (dielectric function, optical absorption, refractive index, reflectivity and optical loss), electronic (electronic band structure, density of states Mulliken's population analysis, charge density of valence electrons) and elastic properties (elastic constants for monocrystalline and polycrystalline states and mechanical stability) of the $CuFeO_2$ compound have been studied in the present study,

In order to describe the fundamental state of the considered system, we first studied the structural properties. However, our values show little over estimation compared with the experimental ones ; It is well known that in general the GGA over estimate the structural parameters, while the LDA underestimates them

Also, the electronic properties such as density of states, charge density and band structures have been presented. The $CuFeO_2$ compound shows an indirect band gap ; we find that the top of the conduction band (CB) is located at the point of symmetry H, and the bottom of the valence band (VB) is located at the point along GM high symmetry axis. Therefore, this compound has an indirect band gap of about 0.630.

Furthermore, we calculated the density of charges into the plan (110) in order to take a general idea about the nature of chemical bonding in the crystalline solid $CuFeO_2$ and to understand briefly the bonds mechanism linking the cations and the anions. The large transfer of charges from the cation to the anion indicates that the anion has a higher electronegativity than that of the cation. Moreover, the Cu-O bond is found much more covalent than the Fe-O bond

In order to study the behavior of the semiconductor $CuFeO_2$ versus incident light, the optical properties such as dielectric function and absorption coefficient, refractive and reflectivity index have been also calculated. We found that the extracted direct optical band gap of $CuFeO_2$ was 0.63. Also, the static dielectric constant $\varepsilon_1(0)$ obtained at zero pressure was about 35.4. Furthermore, there was prominent peak in $L(\omega)$ spectra which represent the characteristic associated with the plasma resonance is located at 36 eV. This pronounced peak of L (ω) corresponds to the beginning of the abrupt decrease of the intensity of R (ω).

On the other hand, we calculated the elastic properties of the $CuFeO_2$ compound such as anisotropic values of elastic constants, Young's modulus E, bulk modulus B, Poisson's ratio to get important information about the mechanics and dynamic properties of the compound. The obtained elastic constants demonstrated the mechanical stability of the Trigonal structure of $CuFeO_2$.

ملخص

هذا البحث قدم في إطار نظرية الكثافة الالكترونية (DFT) اظافة الى نظرية الكمونات الكاذبة (PPs) و الأمواج المستوية (PWs). الخصائص البنيوية , الالكترونية (مستويات الطاقة الالكترونية . خصائص الروابط الكيميائية . كثافة الحالات الالكترونية الجزئية والكلية (TDOS-PDOS) ومخططات التوزيع الالكترونية التكافئية) , المرونة (ثابت المرونة , معامل المرونة والاستقرار الميكانيكي) وكذا الضوئية (معامل العزل , معامل الامتصاص , الانعكاسية و الانكسار) كلها تم حسابها باستعمال تقريب التدرج المعمم (GGA) لطاقة التبادل – الارتباط ببرنامج CASTEP . تم مقارنة النتائج المتحصل عليها مع نتائج تجريبية ونظرية اخرئ.

الكلمات المفتاحية: $CuFeO_2$, Castep, DFT, الأمواج المستوية (PWs) , الكون الكاذب (PPs)

Résumé

Ce travail présente une étude théorique dans le cadre du formalisme de la théorie de la fonctionnelle de la densité (DFT) et l'approche des ultrasoft pseudo-potentiels (PPs) avec les ondes planes (PWs). Les proprétés structurales, électroniques (structure de bades ,des électronique , propriétés des liaisons chimiques les diagrammes de densité d'états «électroniques de valence), élastiques(constantes élastiques , module de compressibilité , module de cisaillement, module de Young , rapport de poisson et stabilité mécanique) et optiques (fonction diélectrique, coefficient d'absorption, réflectivité, indice de réfraction) ont été calculées avec l'approximation du gradient généralisé (GGA) pour l'énergie d'échange-corrélation en utilisant le code castep. Les résultats obtenus sont comparés avec d'autres résultats expérimentaux et théoriques.

Mots clés: $CuFeO_2$, Castep, DFT, Ondes planes (PWs), Pseudo-potential (PPs)

Abstract

This work presents a theoretical study within the formalism of density functional theory (DFT) with pseudopotentials (PPs) and plane waves (PWs) approach. The structural, electronic(electronic band structure, properties of chemical bonds,densty diagrams of total and partial electronic states (TDOS and PDOS) and the valence electronic charge distribution maps) , elastic (elastic constants , bulk modulus, shear modulus , Young's modulus, Poisson rates and mechanical stability) and optical (dielectric function, absorption coefficient reflectivity, refractive index) were calculated with the generalized gradient approximation (GGA) for energy exchange-correlation using castep code. The obtained results were compared with others experimental and theoretical results.

Key Words: $CuFeO_2$, Castep, DFT, Plane wave (PWs), Pseudopotential (PPs)